THE ASTROPHYSICAL JOURNAL, 307:545–563, 1986 August 15

VELA X-1 PULSE TIMING. I. DETERMINATION OF THE NEUTRON STAR ORBIT

P. E. BOYNTON[1] AND J. E. DEETER
Department of Astronomy, University of Washington
AND
F. K. LAMB[2] AND G. ZYLSTRA
Department of Physics, University of Illinois at Urbana-Champaign
Received 1985 July 8; accepted 1986 February 5

ABSTRACT

This is the first of several papers reporting our analysis and interpretation of observations of the pulsed X-ray emission from Vela X-1. Here we consider the interrelated tasks of determining the neutron star orbit and calculating pulse emission times in the rest frame of the source. Our underlying motivation is to utilize this time series for analysis of fluctuations in the pulse emission frequency, which we interpret as noise in the neutron star rotation rate. However, the redness and strength of this noise in Vela X-1 pose a nontrivial complication, because the parameters of the neutron star orbit are estimated by pulse timing and hence are themselves affected by fluctuations in the pulse emission frequency. A second challenge is presented by substantial fluctuations in the Vela X-1 pulse shape that, if ignored, would significantly reduce both the precision of the orbital solution and our ability to study fluctuations in the rotation rate. Our report emphasizes the analysis techniques that have been developed to obtain the most precise orbital solution possible in the face of these difficulties. These techniques are general and may be applied to other pulsars that exhibit substantial fluctuations in pulse shape and frequency, such as Her X-1 and Cen X-3.

Subject headings: pulsars — stars: individual — stars: neutron — X-rays: binaries

I. INTRODUCTION

Fluctuations have been detected in the intrinsic pulse frequencies of most carefully studied rotation- and accretion-powered pulsars (see Cordes and Helfand 1980; Boynton 1981; Henrichs 1983; Inoue 1984). These fluctuations are believed to reflect changes in the rotation rate of the neutron star crust that may be due to torques produced by physical processes either outside or inside the star.[3] In the case of accretion-powered pulsars, the external torque depends on the flow pattern of the accreting plasma and is expected to vary with the accretion rate. The internal torque depends on the nature of the coupling between the liquid interior and the crust. Thus, analysis of fluctuations in the pulse frequency and X-ray flux of an accretion-powered pulsar provides information both about the accretion flow and about the structure of the star itself.

The study of these fluctuations is a particularly powerful way to determine the properties of X-ray stars, because the physics of neutron star rotation has been investigated in detail and is relatively simple compared to much other X-ray source physics. Moreover, stellar rotation rates can be measured precisely with modern X-ray detectors and analysis techniques. Thus, a direct, quantitative confrontation between theory and observation is possible.

This paper is the first of several in which we report in detail the results of our study of the accretion-powered pulsar Vela X-1 using pulse-timing techniques. As discussed by Lamb (1979), Vela X-1 was chosen for this study for three reasons. First, it is widely believed to be a slow rotator (in the sense of Elsner and Lamb 1976, 1977) and is thought to be accreting matter from the stellar wind of its companion (Lamb 1977; Dupree *et al.* 1980; Kallman and White 1982). It therefore provides an example for study that differs in both respects from the previously studied accretion-powered pulsar Her X-1, which is a fast rotator (Elsner and Lamb 1976) accreting from a disk (Pringle and Rees 1972; Lamb, Pethick, and Pines 1973). Second, there were preliminary indications of large fluctuations in the pulse frequency of Vela X-1 from prior studies (see, for example, Becker *et al.* 1978). Finally, as a practical matter, the celestial position of Vela X-1 and the *HEAO 1* observing schedule permitted us to plan and complete a complex series of pointed observations designed specifically to study the noise in the rotation rate.

In addition to the *HEAO 1* data, we also utilized previously recorded but unpublished *OSO 8* observations from 1978 May, and an *SAS 3* observation made in 1979 January specifically to support this study. We have also made use of results from previously published observations.

Our investigation confirms the existence of large, short-term changes in the neutron star spin rate (Nagase *et al.* 1984*a*; van der Klis and Bonnet-Bidaud 1984), in which the sign of the neutron star angular acceleration reverses on time scales as short as 2 or 3 days. We show that these fluctuations in spin rate are consistent with the occurrence of a succession of perturbations that are not resolved by the present observations but have the statistical character of a random walk in pulse frequency. The power density spectrum of the fluctuations in pulse phase produced by such a random walk falls steeply with increasing (analysis) frequency. As a result, most of the power is concentrated at low frequencies. We refer to noise with this type of spectrum as "red noise." Both the change in the apparent secular trend of the pulse frequency from spin-up to spin-down in 1979 and the smaller frequency variations observed on

[1] Also Department of Physics, University of Washington.
[2] Also Department of Astronomy, University of Illinois at Urbana-Champaign; and Visiting Scholar, Stanford University.
[3] For Vela X-1 in particular, the evidence that fluctuations in the pulse frequency on time scales longer than a few days are due to fluctuations in the neutron star rotation rate is compelling (Deeter *et al.* 1986*c*).

shorter time scales are quantitatively consistent with this red noise process. Our results place important constraints on the properties of the neutron star and accretion flow in Vela X-1, as mentioned in a summary of this work published previously (Boynton *et al.* 1984).

In this study, the strength and steepness of the spectrum of fluctuations in the rotation rate of Vela X-1 presented several challenges. Two are specific to determining the pulse-phase time series and the elements of the binary orbit. First, in order to study the behavior of the pulse frequency at the neutron star, it is necessary to remove the apparent variations in the pulse frequency caused by the orbital motion of the neutron star. This is a nontrivial complication, because the estimates of orbital elements are based on the pulse phase observations and are therefore affected by the intrinsic phase variations that we seek to study. In fact, for our observations of Vela X-1, the power density of the red noise in pulse phase caused by fluctuations in the rotation rate of the star dominates that of all other noise by an order of magnitude at the orbital frequency. In dealing with this challenge, we encounter a second, that of estimating the effect of this red noise on the precision of the orbital parameters. By solving this error propagation problem we are able to construct a properly weighted average of all available orbital solutions, including both those determined here and those taken from the literature. This procedure yields a set of orbital elements with nominally minimum uncertainty and therefore provides the "best" approximation to the source rest frame available from the data.

A third challenge, unrelated to fluctuations in the rotation rate, is to reduce the uncertainty in pulse phase caused by fluctuations in pulse shape that are far larger than those attributable to the finite number of photons. This "excess" noise in pulse shape predominantly affects the low harmonics of the pulse waveform. As we discuss in a second paper (Deeter *et al.* 1986*b*, hereafter Paper II), the excess fluctuations in pulse shape are observed to contribute a white component to the spectrum of the noise in pulse phase, even though the spectrum of the shape fluctuations is quite red. We find the noise in phase induced by excess pulse shape fluctuations can be significantly reduced by filtering the pulses prior to the determination of pulse phase. For our highest quality *HEAO 1* data, this technique reduces the variance of the phase estimates by a factor of 4.

This first paper describes the observations, the method used to estimate pulse phase, and the determination of the orbit, emphasizing the elements of our analysis devised to deal with the fluctuations in the stellar rotation rate and the pulse shape variations characteristic of Vela X-1, Her X-1 (Boynton and Deeter 1979; Boynton 1981), and other accretion-powered pulsars. More detailed discussions of some of the techniques used here may be found in Deeter, Boynton, and Pravdo (1981, hereafter DBP) and Deeter and Boynton (1985, hereafter DB). These methods have general applicability to such pulsars and have not previously appeared in the literature.

In Paper II we shall discuss the construction of a record of the pulse frequency at the neutron star and the computation of the power density spectrum of fluctuations in the intrinsic pulse frequency. A full discussion of the implications of this study for the properties of the neutron star and the temporal and velocity structure of the accretion flow will be published elsewhere (Lamb *et al.* 1986).

The remainder of the paper is organized as follows. In § II we summarize the new observations we used, and in § III we describe the method used to handle the interrelated problems of determining the binary orbit and the pulse phases in the source rest frame. We discuss in § IV the mechanics of pulse folding and filtering, the technique used to estimate pulse phase, and our analysis of the uncertainty in the pulse phase. In § V we indicate how we estimated the parameters of the neutron star orbit using only the new data. There we discuss our choice of orbital parameters, which differs in an important way from that of most previous authors. We describe the effect of the observed fluctuations in the rotation rate of the neutron star on estimates of the orbital parameters and discuss the solutions that result from our analysis. In § VI we describe how we combine selected, independent orbital solutions in order to construct a mean orbit for Vela X-1. In § VII we describe the effects of the different noise components encountered in pulse-timing studies, compare different approaches to obtaining orbital solutions from pulse timing, and discuss some of the implications of our results for the design of pulse-timing experiments. In § VIII we summarize the principal results reported here.

II. OBSERVATIONS

New data for this study were obtained from 12 *HEAO 1* pointed observations, utilizing both the A-1 and A-2 experiments, and an *SAS 3* observation. Each of these observations was scheduled specifically for this study, except for one serendipitous pointing. In addition, we were able to use a previously recorded but unpublished block of *OSO 8* data. The *OSO 8* observations provide continuous coverage of a 36 day interval from 1978 May 9 to June 14, while the *HEAO 1* pointings sparsely sample the 61 day interval from 1978 November 1 to December 31. The *SAS 3* observation continuously covers a four-day interval from 1979 January 15 to 19. A journal of the observations is given in Table 1.

The 11 planned, half-day *HEAO 1* observations were deliberately made with octave spacings of 1.5, 3, 6, 12, and 24 days, in order to facilitate construction of a power density spectrum of pulse-phase variations. We shall therefore defer discussion of

TABLE 1

JOURNAL OF OBSERVATIONS

Observation	Time Interval (JD − 2,443,000)	Satellite and Detector
1.....	637.64–672.47	*OSO 8*/module A
2.....	813.82–814.42	*HEAO 1*/A-1 module 3
3.....	837.25–837.74	*HEAO 1*/A-1 module 3
4.....	843.18–843.45	*HEAO 1*/A-2 MED, HED
5.....	850.00–850.46	*HEAO 1*/A-1 module 7
	850.00–850.46	*HEAO 1*/A-2 MED, HED
6.....	855.66–856.15	*HEAO 1*/A-2 MED, HED
7.....	858.93–859.40	*HEAO 1*/A-1 module 7
	858.93–859.40	*HEAO 1*/A-2 MED, HED
8.....	860.43–860.86	*HEAO 1*/A-2 MED, HED
9.....	861.83–862.32	*HEAO 1*/A-2 MED, HED
	862.21–862.26	*HEAO 1*/A-1 module 7
10.....	863.29–863.72	*HEAO 1*/A-2 MED, HED
	863.29–863.72	*HEAO 1*/A-1 module 7
11.....	864.76–865.24	*HEAO 1*/A-2 MED, HED
	864.76–865.24	*HEAO 1*/A-1 molule 7
12.....	867.87–868.42	*HEAO 1*/A-1 module 7
	867.87–868.42	*HEAO 1*/A-2 MED, HED
13.....	873.64–874.17	*HEAO 1*/A-2 MED, HED
14.....	888.40–892.99	*SAS 3*/HTC, XTC

the rationale for this sampling structure to Paper II, where calculation of the power spectrum is described.

The characteristics of the detectors that were used to collect the data are given in Table 2. The count rates from the *OSO 8* and *HEAO 1* detectors were corrected for variations in the illuminated area caused by the motion of the spacecraft. The corresponding correction for the *SAS 3* count rates was unavailable; however, the variations in the illuminated areas of the *SAS 3* detectors occurred on a sufficiently long time scale that the pulse-timing analysis is not affected.

III. METHODOLOGY

The major goals of this paper are to determine the best possible orbit for each data set reported here and to obtain the best possible combined orbit for Vela X-1, using our solutions together with similar orbits available in the literature. This orbit can then be removed uniformly from the pulse-timing observations, leaving insofar as is possible only phase variations inherent to the rotation of the neutron star and the pulse emission process.

In § I we alluded to the problem of obtaining a high-quality orbital solution in the presence of red noise. One method of dealing with random changes in pulse frequency that interfere with the estimation of model parameters is to introduce a polynomial into the fitted function in order to "absorb" such changes to the greatest extent possible. For instance, in analyzing Crab pulsar data, Groth (1975) used this technique to suppress the effect of red noise in rotation on the estimated secular spin-down rate. An auxiliary polynomial is also commonly used to "remove" any secular trend in the pulse frequency when solving for the orbital elements of pulsars in binaries (see Taylor and Weisberg 1982; Ögelman *et al.* 1977; DBP).

Here, we combine these two techniques by including a polynomial of sufficient degree to absorb indiscriminately both random and secular variations in pulse phase, while simultaneously fitting a periodic orbital function. The higher the polynomial degree, the more completely the noise is absorbed; but also, the higher the degree, the more the polynomial interferes with the orbital function. Eventually, the regression problem becomes ill conditioned. By examining the effect on the parameter uncertainties of the residual red noise as well as the white noise introduced by fluctuations in pulse shape, it is possible to choose a polynomial degree that minimizes the overall parameter uncertainties for a given set of data, taking into account *all* sources of noise.

Our method is to partition the data into blocks with durations of several orbits, separately derive an orbit for each block, and then average the resulting ensemble of orbital elements. This "local" approach seems intuitively appealing, particularly when one is confronted with data containing large gaps, and has several substantial advantages over the alternative of a single "global" orbital solution obtained directly from all available data. Because the method is a general one applicable to other noisy pulsars, we discuss it in some detail in § VII.

In the case of our Vela X-1 data, the sampling structure suggests a natural partitioning into two blocks: (1) the *OSO 8* observations of 1978 May and (2) the *HEAO 1* and *SAS 3* set begun in 1978 November. Each block effectively covers about four and nine binary orbits respectively, while the gap between them is approximately 16 orbits. An orbital solution was obtained for each block of data by first choosing provisional values for all important parameters, such as the pulse frequency and the elements of the binary orbit. Short intervals of flux data were then folded at the (constant) provisional pulse frequency in the frame that is comoving with the source according to the provisional orbit. The resulting submaster pulse templates were used to determine the residual pulse phases, relative to the provisional pulse frequency and binary orbit, by comparing them with a master template. Finally, the residual phases were analyzed for corrections to the provisional values of the parameters, while simultaneously fitting an appropriate noise-absorbing polynomial (no such polynomial was included during the pulse-folding process).[4]

This approach is close in spirit to that discussed by Epstein (1977), sharing with it several important features. First, time in the source rest frame is taken correctly as the independent variable both for computing the orbital term and for expanding the pulse phase as a Taylor's series in order to determine

[4] For the sake of brevity, from now on we refer to residual pulse phases simply as pulse phases. The precise meaning of the term "pulse phase" will change as the analysis proceeds, but at any given point the meaning should be clear from the context.

TABLE 2

CHARACTERISTICS OF THE DETECTORS USED[a]

Satellite and Detector	Time Resolution (s)	Detector Area (cm^2)	Nominal Energy Ranges (keV)
OSO 8/module A	10.5[b]	263	2.0–30.0
HEAO 1/A-1 module 3	0.64	1650	0.7–1.3, 1.3–2.0, 2.0–6.0, 6.0–11.3, 11.3–43.3[c]
			0.7–1.3, 1.3–2.0, 2.0–6.2, 6.2–12.1, 12.1–47.5[d]
HEAO 1/A-1 module 7	0.64	1900	0.1–0.6, 0.6–2.1, 2.1–8.3, 8.3–15.4, 15.4–18.9
HEAO 1/A-2 MED	5.12	820	2.0–20.0
HEAO 1/A-2 HED	5.12	820	2.0–7.5, 7.5–60
SAS 3/HTC	0.83	80	1.0–2.5, 2.5–5.0, 5.0–10.0
SAS 3/XTC	0.83	115	8.0–18.0, 18.0–27.0, 27.0–35.0

[a] Descriptions of the satellites and detectors are available as follows: *OSO 8*, Serlemitsos *et al.* 1976; *HEAO 1* A-1, Chubb 1976; *HEAO 1* A-2, Rothschild *et al.* 1979; *SAS 3*, McClintock *et al.* 1976, Buff *et al.* 1977.

[b] Rotation period of the satellite. The detector is skewed relative to the spin axis; the time on source for each rotation and the effective time resolution are both ~2.5 s.

[c] Energy ranges for observation 2.

[d] Energy ranges for observation 3.

the rotation frequency and its derivatives. Second, since the Doppler shift specified by the provisional orbit has already been removed, pulse folding can be conducted at constant pulse frequency without smearing the pulse shape. Finally, estimating the small corrections to the provisional orbital parameters is essentially a linear problem. If the corrections are not small, the entire procedure can be repeated with corrected values of the parameters until the desired precision is attained.

IV. ESTIMATION OF PULSE PHASES

As the first step in implementing this methodology, we transformed all times of observation to times at the solar system barycenter. The subsequent provisional transformation to time measured in the frame of the neutron star was based on an orbit for Vela X-1 computed as a joint fit to 1975 June–July and 1978 November data from *SAS 3* by Rappaport, Joss, and Stothers (1980). This solution included a term for $\dot{\omega}$, the apsidal advance rate, and yielded a value consistent with zero. For the purpose of pulse folding, we set $\dot{\omega}$ equal to zero. The pulse smearing caused by inaccuracy in the provisional orbit and by variations in pulse frequency was found to be no more than 1 s for the *OSO 8* data (12 hr superposition span), and no more than 0.1 s for the *HEAO 1* data (1 hr span). The resulting attenuation in harmonic amplitude becomes significant at about the 20th and 200th harmonics respectively, well beyond the point at which the harmonics disappear into noise.

Pulse phases were estimated using a version of the common method of pulse folding and cross-correlation. We first formed submaster templates by pulse folding. The shape of these folded pulses varied far more than expected from photon statistics alone, and these excess fluctuations in pulse shape did not have the character of white noise (equal power in the fluctuation of each harmonic component of the pulse). As discussed by DB, optimal estimation of pulse phase in this situation can be achieved by filtering the folded pulses, using a filter whose properties are determined by the spectrum of the noise in pulse shape. By adopting this modification of the basic cross-correlation scheme, we were able to improve substantially the precision of the phase estimates derived from the high-quality *HEAO 1* data.

In §§ IV*a*–IV*d* we first discuss the construction of submaster and master templates and the cross-correlation technique for estimating pulse phases. Next we introduce a filtering procedure designed to decrease the uncertainty in the phase estimates by reducing the influence of the noisiest harmonics. We then describe how we evaluate the effectiveness of filtering by comparing the measured uncertainties in phase estimates obtained from filtered and unfiltered pulses. Finally, we use this information to tie together phases from different instruments and consolidate phases from different energy channels to produce a single, final series of pulse-phase estimates and associated uncertainties.

a) Construction of Pulse Templates

Submaster templates were formed for each energy channel of each detector by folding short segments of the count rate data using constant provisional pulse periods of 282.793 s for the 1978 May data and 282.7492 s for the 1978 November–1979 January data. In the case of the *HEAO 1* data, one submaster was constructed from the data acquired in a 1 hr interval during each satellite orbit. In the case of the *SAS 3* and *OSO 8* satellites, which had much lower count rates, we used data spanning 6 and 12 hr intervals respectively in forming each submaster.

The submaster templates were constructed by distributing the count rate data into 64 equal time bins. Binning on this small interval over-resolves our data in the sense that noise completely dominates structure on the bin-to-bin time scale. No information is lost by over-resolution, however, and we discuss in § IV*b* reduction of the resolution to an optimum value. Each integration interval overlapped one to three bins. The number of counts in each integration interval was therefore distributed pro rata among the bins overlapped.

Once the count rate data had been folded to produce submaster templates, these templates were expanded in a Fourier series, as described by DB. Depending on the application, either this harmonic representation or a time domain description based on binning was used for subsequent analysis. In the following discussions we take advantage of whichever representation lends greater clarity.

Master templates used in the cross-correlation were formed for each energy channel of each detector by superposing the corresponding submaster templates. This superposition required prior alignment of the submaster templates to much greater accuracy than that provided by the pulse ephemeris used in constructing the submasters. We therefore adopted a two-step procedure.

As the first step, we formed a temporary master template for each experiment (*OSO 8*, *HEAO 1*, and *SAS 3*) by a "bootstrap" method, using only the energy channel with the highest counting rate. In this method, cross-correlation was used to determine the phase of each submaster template formed from the selected high–count-rate channel relative to the partial master pulse formed from the previous submasters. This phase was used to align the submaster with the partial master, and these pulses were then combined to form a new, updated partial master. The final partial master—composed of all the submasters—was adopted as the temporary master template for that energy channel.

In the second step, we refined this superposition procedure to construct final master pulses for every energy channel of each experiment. To begin this step, we conjointly aligned concurrent submaster templates from the various energy channels of each experiment. This alignment was based on the single phase offset obtained by cross-correlating the submaster from the selected high–count-rate channel with the corresponding master template for that experiment. In forming the *OSO 8* and *SAS 3* master templates, we utilized all the aligned submaster templates. For the *HEAO 1* master templates, we used only those submasters corresponding to satellite orbits with concurrent A-1 and A-2 data. This procedure ensured that there were no avoidable phase shifts between the master templates corresponding to different energy channels of the same experiment. The three *HEAO 1* A-2 master templates formed by averaging the aligned submasters are shown in Figure 1.

The offset between a submaster and its corresponding master template was taken as the phase shift necessary to produce a maximum in their cross-correlation, which is formally equivalent to solving for a minimum variance superposition of the two templates (DB). To compute the cross-correlation, we assume that each submaster $g(\phi)$ is a scaled and shifted version of the master template $h(\phi)$, that is,

$$g(\phi) = ah(\phi + \tau) , \quad (1)$$

for some a and τ. We adopt units in which $h(\phi)$ is dimensionless and a is the mean count rate. The templates obtained by pulse-folding actual data are defined only at the discrete set of points

$$\phi_j = \frac{j}{n} P , \quad j = 0, \ldots, n-1 , \quad (2)$$

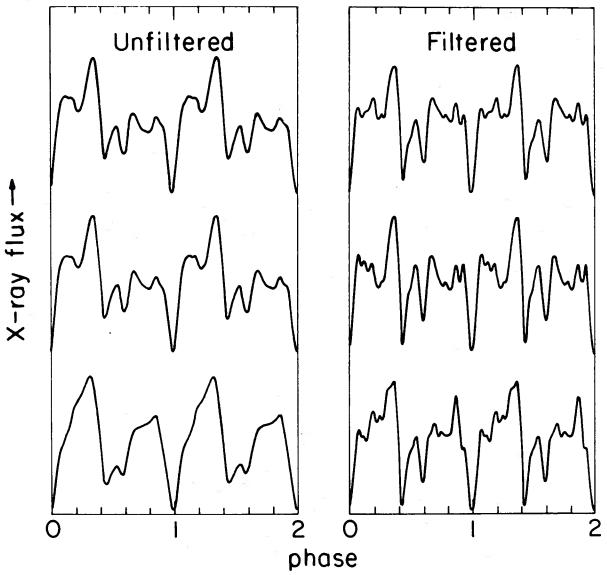

FIG. 1.—(*left*) *HEAO 1* master pulse templates constructed from Fourier representations truncated at the 16th harmonic. From top to bottom, these pulses are derived from the 2–20, 2–7.5, and 7.5–60 keV energy channels of the *HEAO 1* A-2 observations of Vela X-1. (*right*) Filtered versions of the master templates shown on left.

where P is the reference pulse period and n is the number of bins in a pulse period. We adopt the abbreviations

$$g_j = g(\phi_j), \quad h_j = h(\phi_j), \quad j = 0, \ldots, n-1 \tag{3}$$

and estimate the pulse offset from the maximum in the discrete cross-correlation

$$C_k = \sum_{j=0}^{n-1} g_j h_{j+k}, \quad k = 0, \ldots, n-1. \tag{4}$$

The phase offset is then given by inverse interpolation on the discrete cross-correlation near the maximum at bin K,

$$\hat{\tau} = \frac{P}{n}\left[K - \frac{C_{K+1} - C_{K-1}}{2(C_{K+1} - 2C_K + C_{K-1})}\right]. \tag{5}$$

In this formula a positive $\hat{\tau}$ denotes an *early* pulse arrival (negative $O - C$).

Because the observations made in 1978 May were treated independently from those made in 1978 November–1979 January, no attempt was made to align master templates formed from these two blocks of data. However, we wanted to consider the *SAS 3* and *HEAO 1* data as part of the same time series. To do so, we had to determine the relative phase offset between the masters for the two sets. The *SAS 3* masters were aligned with the *HEAO 1* masters by cross-correlating one master template formed with data from an *HEAO 1* energy channel with one formed with data from an *SAS 3* energy channel. The two master templates that most closely matched each other in shape were those derived from the *HEAO 1* A-1 15.4–18.9 keV channel and the *SAS 3* XTCA (8–18 keV) channel. We found that the phase of the *SAS 3* master relative to the *HEAO 1* master was -9.2 ± 0.5 s. Consequently, -9.2 s was added to all phases derived from the *SAS 3* data.

b) Filtering of Templates

The uncertainty in the pulse-phase estimate derived from a given submaster may be due to a variety of causes but is bounded below by the uncertainty induced by the noise in pulse shape due to photon statistics. This error propagation problem has been discussed in several settings (Groth 1975; Downs and Reichley 1983; DB). In the notation of the present paper, the variance in the phase estimate due to white noise in the flux time series is

$$\sigma_\tau^2 = \mathrm{var}\,(\hat{\tau}) = \frac{\sigma_a^2/a^2}{P^{-1}\int_0^P [h'(\phi)]^2 d\phi}, \tag{6}$$

where σ_a^2 is the variance in the mean count rate a.[5] For photon statistics, $\sigma_a^2 = a/\beta T$, where β is the ratio of detector "live" time to the total time span T over which the pulse is folded.

It is well known that the Vela X-1 pulse shape varies greatly, even from pulse to pulse (see, e.g., Staubert *et al.* 1980). For high–count-rate data, these variations substantially exceed those due to photon statistics. The pulse shapes for the *HEAO 1* data, for example, show a mean-square scatter ~ 20 times that expected from photon statistics alone. For such data, it is the excess fluctuations in the pulse shape that limit the precision of the pulse phase estimates. Because the excess noise in the Vela X-1 pulse shape is not white, filtering the pulse templates before performing the cross-correlation analysis substantially improves the precision of the pulse estimates derived from the *HEAO 1* data.

The reason for this improvement can be understood as follows. Each phase estimate obtained using the cross-correlation technique may be regarded as a weighted average of the phases of the individual harmonics that comprise the submaster template in question, with weights chosen to be optimum for white pulse-shape noise (equal variances in all the harmonic coefficients of the template). Thus, a pulse phase estimate obtained by cross-correlating a given submaster template with the appropriate master template has minimum variance only if the shape noise in the submaster template is white (DB).

Viewing the problem in this way suggests a procedure that will improve the precision of the phase estimates when the pulse-shape noise is *not* white but nevertheless consists of independent harmonic components: alter the weighting of the harmonic coefficients in the templates so that the pulse shape noise is *made* white. This procedure alters the relative amplitudes of the harmonics in the templates while leaving their relative phases unchanged. It may be implemented in the time domain by convolving the templates with a filter whose transfer function is proportional to $1/S(f)$, where $S(f)$ is the power spectral density of the pulse-shape noise. We assume that the shape noise can be written as independent harmonic components, in which case filtering is a statistically correct procedure to reduce the scatter in the phase estimates (DB). However, we did not directly verify that the harmonics are independent in the present data analysis. Consequently, our method of flattening the power spectrum of the pulse-shape fluctuations does not guarantee that they are made truly white. The filtering procedure did, however, result in a significant improvement in the precision of pulse timing for the *HEAO 1* data presented here.

[5] By employing a harmonic representation of the mean pulse shape (DB), we may write $h(t) = \sum_k H_k \cos k(\Omega t - \theta_k)$, where Ω is the pulse frequency and the sum include all harmonics with statistically significant amplitudes. From eqn. (6) one can then see how the harmonic content and frequency of the pulse affect the propagation of fractional fluctuations in amplitude into fluctuations in pulse phase, $\sigma_\tau^2 = 2(\sigma_a/a)^2(\Omega^2 \sum_k k^2 H_k^2)^{-1}$.

The tapering of the filter at high frequencies is just as important as its shape at low frequencies. In order to minimize the variance of the phase estimates, it is necessary to discard harmonic terms in the master template that do not stand out above noise (see DB). Since the amplitudes of the harmonics in our templates decrease rapidly with increasing harmonic number, simply setting the response of the filter to zero at the first harmonic that falls below noise and at all higher harmonics is an adequate tapering. We therefore introduced a cutoff at the 12th harmonic in the filter applied to the *OSO 8* data and at the 16th harmonic in the filter applied to the *HEAO 1* data. By retaining only lower harmonics in the Fourier representations of the pulse wave forms, we also avoid a potential bias in the phase estimates caused by a "noise spike" in the cross-correlation arising from the *auto*-correlation of each submaster with its copy in the master template (DB).

We determined the power spectrum of the pulse-shape fluctuations from the residual pulses, where a residual pulse is defined as the difference between an aligned and scaled version of a submaster pulse and the corresponding master pulse,

$$\Delta\tilde{g}(\phi) = \frac{1}{a}\, g(\phi - \hat{\tau}) - h(\phi)\,. \tag{7}$$

Averaging the squares of the Fourier coefficients of these residual pulses, harmonic by harmonic, then provides the discrete power spectrum of the shape noise at harmonics of the pulse frequency. Power spectra of the pulse-shape noise and also of the pulse shape itself (as defined by the master template) were constructed separately for each energy channel. In Figure 2 the power density spectrum of the *HEAO 1* A-2 master template (2–7.5 keV) is shown along with the corresponding spectrum of pulse-shape fluctuations. Note that the spectrum of shape fluctuations is quite red, indicating that the lowest harmonics of the pulse shape are the most variable.

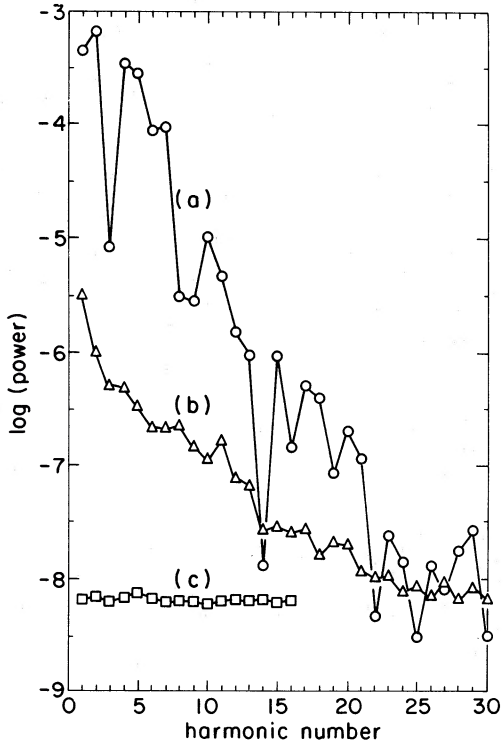

FIG. 2.—(*a*) Squared Fourier transform of the master pulse formed from the *HEAO 1* A-2, 2–7.5 keV data. (*b*) Average of the squared Fourier transforms of the residual pulses for the same data. This curve has been divided by 69 (the number of submasters) to provide an indication of the noise level in the master pulse. Therefore, the harmonics in the master pulse which stand out above noise can be determined by inspection. (*c*) Average squared Fourier transforms of the residual pulses for the 2–7.5 keV data after two iterations of the filtering procedure designed to flatten the spectrum, as described in the text.

From each power spectrum we can construct the symmetric cosine filter

$$F(\phi) = \sum_{k=1}^{m} [S(f_k)]^{-1/2} \cos 2\pi f_k \phi\,, \tag{8}$$

wherein m is the maximum harmonic used, $f_k = k/P$ is the frequency of the kth harmonic of the pulse frequency, and ϕ is the pulse phase in seconds. Recomputation of the pulse-shape noise for the filtered submaster and master templates should yield a power spectrum which is reasonably flat. We discovered, however, that the spectrum for the filtered pulses was still slightly red, due to the use of a nonoptimum scale factor a based on the unfiltered pulses (see eq. [7]). A second-pass filter, based on the power spectrum constructed from the filtered pulses using revised scale factors, produced twice-filtered pulses that possess an adequately flat shape noise power spectrum (see Fig. 2).[6] The three filtered master templates for the *HEAO 1* A-2 experiment are shown in Figure 1, along with their unfiltered predecessors.

Finally, each filtered submaster was cross-correlated with the corresponding filtered master (for each energy channel and experiment), and phase estimates were subsequently determined through the application of equation (5). These pulse phase estimates have minimum variance (over all possible linear filters) under the assumptions stated for the pulse shape noise. Again, rather than attempt to test the validity of these assumptions in detail, principally whether the phases of pulse-shape harmonics are truly independent, we chose to examine directly whether filtering improves the stability of phase estimates by evaluating their local scatter. In § IV*c* we show that such filtering does markedly improve the precision of phase estimates derived from the high-quality *HEAO 1* data but does not improve the precision for the *OSO 8* and *SAS 3* data, where the white pulse-shape noise due to the finite number of photons is much stronger.

c) Phase Uncertainties and Evaluation of Filtering

A measure of the uncertainty of the pulse phase estimates is needed in order to evaluate whether filtering provides any improvement. In this discussion it is important to distinguish the spectrum of fluctuations in pulse *shape* from the spectrum of fluctuations in pulse *phase* induced by the pulse-shape fluctuations. We show in Paper II that even though the power density of the fluctuations in pulse shape declines with harmonic number (i.e., is red), the *observed* spectrum of fluctuations in pulse phase *induced* by the pulse-shape noise is white, at least on time scales longer than the template-folding interval (1–12 hr). Thus, the induced fluctuations in pulse phase are

[6] We believe that the empirically determined power spectrum of the pulse-shape noise adequately approximates the true spectrum for the purpose of improving pulse timing through pulse filtering. There is, however, the possibility that the spectrum may be distorted in the process of aligning and scaling the sample pulses. For instance, if a single harmonic dominates the pulse, almost all information about noise in that harmonic is lost in the process of aligning and scaling the pulse. When several harmonics contribute to the pulse shape, as in Vela X-1, there will still be a loss in noise power, but now the reduction will be divided among the largest harmonics. For the spectrum shown in Figure 2, we estimate that the distortion from alignment and scaling is at most 30% for the sixth and seventh harmonics, and is smaller elsewhere. This is a relatively small effect, given the 2.5 decade range in noise power density. Even so, this distortion could be avoided by using other methods, which align and scale the pulses collectively rather than individually.

inferred to be uncorrelated from one submaster to the next. We therefore chose as a measure of the uncertainty of the individual phase estimates the rms deviation of short segments of the pulse-phase time series from a local straight-line fit. By using segments short enough, we ensured that the scatter was dominated by the fluctuations in pulse phase induced by pulse-shape noise, rather than by the fluctuations produced by the red noise in the neutron star's rotation rate.

In order to calculate the rms deviations from local straight-line fits, we had to choose appropriate weights for the individual phase estimates. If photon statistics were the only source of pulse-shape fluctuations, it would be proper to weight the phase estimates by inverse Poisson variances (see discussion of eq. [6]). However, the presence of pulse-shape noise substantially in excess of that due to photon statistics made the use of Poisson weights questionable. As an alternative, we considered assigning each phase estimate equal weight, which would be appropriate for stationary processes that produce fractional fluctuations in harmonic amplitudes which are independent of the number of detected photons. On comparing the results using uniform weighting with those based on Poisson weighting, we found that neither scheme was clearly favored.

In the end, we adopted uniform weighting in analyzing all data sets because of its simplicity. The resulting phase uncertainties are shown in Table 3. The first of them (σ_p) shows the average expected error due to the finite number of photons in the template for the various energy channels of each experiment. The next columns compare the empirical uncertainties derived from the observed scatter of phase estimates from local, straight-line fits for unfiltered (σ_0), once-filtered (σ_1), and twice-filtered (σ_2) submaster templates. These results show that filtering the templates substantially improves the precision of the phase estimates derived from the *HEAO 1* data, where the variance was reduced by as much as a factor of 4 for the highest quality data. In contrast, filtering did not significantly improve the precision of the phase estimates derived from the lower quality *OSO 8* and *SAS 3* data. This outcome is to be expected, since pulse-shape noise due to the finite number of photons is more important in the *OSO 8* and *SAS 3* data, than not in the *HEAO 1* data.

d) Final Phase Estimates and Uncertainties

Only a single set of phase estimates could be derived from the 1978 May *OSO 8* data, since the data from this satellite were not energy-resolved. On the other hand, from three to six independent sets of phase estimates were derived from the 1978 November–1979 January *HEAO 1* and *SAS 3* data, since the data that we obtained with these satellites were partitioned both by detector and by energy channel. In the latter case, final phase estimates for each experiment as a whole were formed by averaging the phase estimates derived from the individual energy channels of the experiment, using weights proportional to the reciprocal of the point variance assigned to each energy channel from the local straight-line fits described above. The weights chosen are listed for reference in Table 3. One second was subtracted from the *SAS 3* phases to compensate for the leap second introduced in UTC at 1979 January 1.0, in addition to the correction for the time offset between the *HEAO 1* and *SAS 3* master pulses (see § IV*a*).

The uncertainty of the final phase estimates could not be estimated correctly by simply adding in quadrature the uncertainties of the individual phase estimates that were averaged to form them, because fluctuations in the pulse shape in one energy channel in excess of those due to photon statistics are likely to be correlated with excess fluctuations in the pulse shape in other energy channels. We therefore estimated the uncertainty of the pulse phases derived from each experiment as a whole in the same way that we estimated the uncertainty

TABLE 3

EVALUATION OF THE EFFECT OF FILTERING ON PHASE UNCERTAINTIES

SATELLITE	ENERGY RANGE (keV)	rms RESIDUALS[a] (s)				RELATIVE WEIGHT	σ_{ave}[b] (s)
		σ_p	σ_0	σ_1	σ_2		
OSO 8	2–30	0.59	1.34	1.28	1.33	1.00	1.34
HEAO 1/A-1[c]	2.1–8.3	0.14	1.11	0.86	0.93	0.53	0.56[d]
	8.3–15.4	0.19	1.02	0.67	0.67	1.00	
	15.4–18.9	0.28	1.20	0.90	0.89	0.59	
HEAO 1/A-2	2–20	0.15	1.01	0.66	0.63	0.61	0.50
	2–7.5	0.15	0.94	0.53	0.49	1.00	
	7.5–60	0.21	1.08	0.86	0.83	0.35	
SAS 3[e]	2.5–5	0.49	1.28	1.32	1.29	0.44	0.78
	5–10	0.45	1.16	1.33	1.37	0.53	
	8–18	0.36	0.84	0.67	0.81	1.00	
	18–27	0.59	1.22	1.31	1.46	0.30[f]	

[a] σ_p is the average uncertainty in the phase of each submaster pulse due to counting statistics (finite number of photons). σ_0, σ_1, and σ_2 are the empirically determined mean uncertainties (derived from observed scatter of phase estimates for local straight-line fits) for unfiltered submasters and once- and twice-filtered submasters, using filters constructed to whiten the pulse shape noise.

[b] Empirically determined mean uncertainty in the final phase estimates, which are obtained by averaging the phase estimates for the energy channels of each experiment, using the weights in the previous column.

[c] Because of low count rates, the lowest two energy channels of the A-1 experiment were not used for pulse timing.

[d] Excluding 1978 Nov. 1 data.

[e] Because of low count rates, the lowest energy (1.0–2.5 keV) channel of the HTC and the highest energy (27–35 keV) channel of the XTC were not used for pulse timing.

[f] This weight should be 0.51, but by a transcription error was reduced to 0.30. The effect of this incorrect weighting on the final phase estimates is not very important, and reaveraging was not performed.

of the pulse phases derived from a single energy channel; namely, by computing the rms deviation of the final phase estimates from local straight-line fits (again, using uniform weights). The phase estimates derived from the 1978 November 1 data showed an unexplained large scatter and so were excluded from this computation. The results for all experiments are shown in the last column of Table 3. Because the uncertainties of the phase estimates derived from the A-1 and A-2 data are so similar, we combined these two sets of phase estimates and assigned a common point variance of 0.51 s based on the rms scatter of the phases from local straight-line fits.

The phase estimates derived from the three final groupings of the data are shown in Figure 3. The sinusoidal phase variation with a period of ~ 9 days apparent in this figure is due to the inaccuracy of the provisional orbit. This variation disappears when the more accurate mean orbit derived in § VI is used.

V. DETERMINATION OF THE NEUTRON STAR ORBIT

Our goal is to determine orbital parameters with the highest possible precision given the data available and to make a realistic estimate of their uncertainty. In Vela X-1, the pulse phase wanders significantly as a result of the noise in the rotation of the neutron star. This noise is red in the sense that the power density of the phase residuals is much greater at low frequencies than at high frequencies and is consistent with a random walk in pulse *frequency* (Paper II). The noise in pulse *phase* can therefore be described as the first integral of a random walk or, equivalently, the second integral of a white noise process. We therefore call this type of noise *second-order* red noise (Deeter and Boynton 1982). This noise in the rotation rate dominates all other contributions to the uncertainties in the orbital parameters for our Vela X-1 data; consequently, a realistic assessment of its contribution to the uncertainty of the orbital parameters is essential.

For the reasons given in §§ III and VII, we determined separate orbital solutions for the 1978 May data and for the data beginning in 1978 November. The presence of the red noise in rotation motivated us to shorten the second data set for the purpose of calculating the orbit. The initial pointing in this set (1978 November 1) is separated from the next by 23 days, which allows a sizable uncertainty in the pulse phase to accumulate between these two observations and thus effectively decouples the initial pointing from the local emphemeris. The same is true of the 1979 January *SAS 3* data, which are separated by 14 days from the final *HEAO 1* observation on 1978 December 31. Inclusion of either point at the ends of the entire 70 day data span would not significantly improve the local orbital solution. Therefore, we chose to include only the observations from the 12 pointings during the 37 day interval from 1978 November 24 to December 31 in our determination of the local orbit based on the second data set.

In carrying out the least-squares analysis described below, we assigned the phase estimates within each data set the same weight, equal to the inverse of the point variance obtained from the local scatter in pulse phase in the manner discussed in

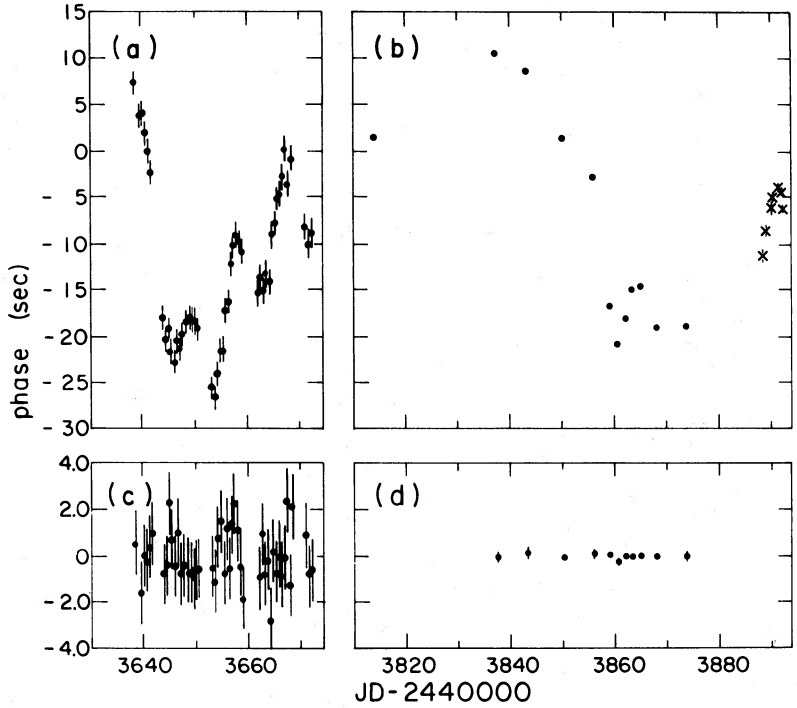

FIG. 3.—(*a*) Residual phases in seconds, with respect to the provisional orbit and the provisional local pulse frequency, for the 1978 May (*OSO 8*) data. The vertical bars correspond to the estimated uncertainty of 1.34 s. (*b*) Residual phases, with respect to the provisional orbit and the provisional pulse frequency, for the 1978 November–December data from *HEAO 1* (*filled circles*) and the 1979 January data from *SAS 3* (*crosses*). Each point is an average of the residuals derived from 12 hr of data. The vertical bars on the *SAS 3* data indicate the uncertainty of the averaged point, based on individual phase uncertainties of 0.78 s. The phase uncertainties of the averaged *HEAO 1* data points, based on individual phase uncertainties of 0.51 s, are too small to be seen in this panel. (*c*) Residual phases, with respect to the best-fit local orbit given in Table 5 and a fifth-degree polynomial, for the 1978 May data. Note that the vertical scale is a factor of 2.5 larger than that of (*a*). (*d*) Residual phases, with respect to the best-fit local orbit given in Table 5 and a sixth-degree polynomial, for the 1978 November–1979 January data. The segments at either end of the data set (1978 November 1 and 1979 January) were not included in the local fit for the orbit. Consequently the residuals for these two segments were very large and are not shown. Note that the vertical scale is a factor of 2.5 larger than that of (*b*).

the previous section. The equivalent standard deviations are 1.34 s for the 47 phases in the 1978 May data set and 0.51 s for the 110 phases in the 1978 November–December set.

a) *Choice of Orbital Parameters*

Factors affecting the choice of orbital parameters in pulse-timing studies have been discussed previously by DBP. The main point made in their Appendix A is that only a term of order e distinguishes an orbit with small eccentricity from a circular one. That is, an orbit with small eccentricity is approximated by a sum of first and second harmonic terms with an amplitude ratio of $e/2$. While the amplitudes of these two terms are determined with comparable precision even in the presence of the red noise being confronted in this study, the precision to which the phase (or epoch) of each term is determined depends on the *fractional* uncertainty in the respective amplitudes. For this reason, the uncertainty in epoch of the first harmonic (epoch of mean longitude) is smaller by a factor of $e/2$ than the uncertainty in the epoch of the second harmonic (time of periapsis). The time of periapsis T_ω is therefore poorly determined, and a better choice for orbital fiducial is an epoch in mean longitude. As advocated by DBP, we adopt for our orbital epoch the time when the mean longitude is $\pi/2$ and, following van der Klis and Bonnet-Bidaud (1984), denote it by $T_{\pi/2}$. For a circular orbit, $T_{\pi/2}$ corresponds to the time of *geometric* conjunction, which differs from the time of *apparent* conjunction (mideclipse) by the light travel time correction given by DBP. For an orbit with finite eccentricity, an accurate description of $T_{\pi/2}$ is given by the awkward phrase "time of conjunction in mean longitude." Lacking a better term, we shall refer to $T_{\pi/2}$ as simply "the orbital epoch."

We note also that for small eccentricity the determination of ω, the longitude of periapsis, suffers from the same adverse propagation of error as does the determination of T_ω. Furthermore, estimates of these two quantities from the same data are highly correlated because both depend on the phase of the second harmonic. By definition, $T_{\pi/2}$ is given by their difference:

$$T_{\pi/2} = T_\omega - \frac{P_{\rm orb}}{2\pi}\left(\omega - \frac{\pi}{2}\right). \tag{9}$$

Consequently, the much more accurate $T_{\pi/2}$ can be recovered from conjointly determined T_ω and ω. In the following section we make this conversion for orbital solutions taken from the literature.

Aside from the orbital epoch, the other orbital parameters that can be determined locally are the projected semimajor axis $(a/c)\sin i$, eccentricity e, and longitude of periapsis ω. We did not attempt to determine the orbital period or its rate of change locally, preferring to determine these parameters from an analysis of all available orbital epochs.

b) *Effect of Red Noise on the Orbital Parameters*

In assigning uncertainties to the orbital parameters, we used a method based on the sampling function formalism developed by Deeter (1984) to define the propagation of error. We also used this error analysis scheme to select the degree of the noise-absorbing polynomial included in each orbital solution. Here we briefly review this method. Further details are provided in the Appendix.

When parameters are determined in the usual way, by fitting a function to data using the method of least-squared residuals, it is tacitly assumed that the noise in the observations is accurately described by a data covariance matrix. The inverse of this matrix provides a suitable weight matrix for the data points, and the uncertainties in the parameters are then obtained by inverting the normal equations. As discussed in the Appendix, this method is not directly applicable to data containing red noise, since the data covariance matrix is not positive definite and therefore does not yield an acceptable data weight matrix. For this reason, we have adopted an ad hoc approach.

According to the methodology outlined in § III, we absorb noise on long time scales by fitting a suitable polynomial, weighting the individual pulse phases according to their estimated residual variances. We can then use the procedure discussed in the Appendix to estimate the uncertainties in the orbital parameters arising from the particular kind of red noise in pulse phase observed in Vela X-1. By also including the uncertainties caused by the white noise in pulse phase induced by the fluctuations in pulse shape, we can choose the degree of the auxiliary polynomial to minimize the *combined* uncertainties. This criterion differs from the commonly accepted one of fixing the polynomial degree at the point where the phase residue stops decreasing. Although the polynomial degrees specified by these two criteria are quite similiar for the present data, our method relies directly on the parameter uncertainties themselves, which are estimated by a formally correct error propagation formula.

A possible difficulty in obtaining the correct parameter covariance matrix is that the least-squares problem for the orbit plus polynomials is nonlinear and must be solved by iteration. In the case at hand, however, the nonlinear terms are small compared to the parameter errors. Therefore, we accept the covariance matrix for the final parameter adjustments as the covariance matrix for the parameters themselves, as is done in the case of nonlinear least-squares applied to data containing white noise. Since the problem is strictly linear in the polynomial coefficients, they are not explicitly considered in the following discussion of the linearized orbital solution.

To linearize this least-squares problem, we used an approximate expression for the change in the orbital time delay $\Delta t_{\rm orb}$, in terms of small changes in the orbital parameters (cf. DBP), namely,

$$\Delta t_{\rm orb} = \Delta a_1 \cos l + \Delta b_1 \sin l + \Delta a_2 \cos 2l + \Delta b_2 \sin 2l\,. \tag{10}$$

Here l is the provisional mean longitude, measured from the ascending node. This approximation retains only first-order terms in the eccentricity and involves only the first and second harmonics of the mean orbital motion. To first order in the eccentricity, the corrections to the orbital parameters are related to the coefficients in equation (10) by the expressions

$$\begin{aligned} \Delta a_1 &= -\frac{2\pi x}{P_{\rm orb}}\Delta T_{\pi/2}\,, \quad & \Delta b_1 &= \Delta x\,, \\ \Delta a_2 &= -\tfrac{1}{2}x\Delta g\,, & \Delta b_2 &= \tfrac{1}{2}x\Delta h\,, \end{aligned} \tag{11}$$

where $x = (a/c)\sin i$ is the projected semimajor axis, $\Delta T_{\pi/2}$ is the local correction to the orbital epoch, $P_{\rm orb}$ is the provisional orbital period, and $g = e\sin\omega$ and $h = e\cos\omega$ are the Cartesian equivalents of the eccentricity e and longitude of periapsis ω. The harmonic coefficients Δa_1, Δb_1, Δa_2, and Δb_2 are all expressed in the same units; consequently, their uncertainties are identical for uniform sampling and white noise in

pulse phase. These uncertainties continue to be the same order of magnitude even for nonuniform sampling and nonwhite noise, making it particularly easy to compare the changes in the uncertainties of the harmonic coefficients as the polynomial degree is varied. This is not true for the parameter corrections themselves, which are expressed in a variety of units.

With this error propagation scheme, it is possible to determine the contribution to orbital parameter uncertainties from the noise in rotation. However, the properties of this noise cannot be determined completely unless the orbit is known accurately. In order to break this apparent circularity, we first made a provisional determination of the type and strength of the noise at frequencies lower than the orbital frequency. We found that at these frequencies the noise was adequately modeled by second-order red noise in pulse phase, with a random-walk strength of 8×10^{-19} rad^2 s^{-3} (see Paper II).

To select the optimum polynomial degree, we solved the linearized least-squares problem nine times for each data set, including in turn first through ninth degree polynomials. In each case we computed the expected variance in each of the orbital parameters due to the white noise in pulse phase contributed by pulse shape fluctuations as well as that due to second-order red noise in pulse phase with the strength given above. Since these two kinds of noise are independent, we can add their variances to obtain a total variance for each parameter.

Table 4 shows the behavior of the total uncertainty in the orbital parameters σ_t as polynomials of increasing degree are included. For both data sets, the σ_t's of all the parameters generally decline as the degree of the polynomial is increased. After a certain point, however, the subsequent decline is comparatively modest. On this basis we chose to include a fifth-degree polynomial in analyzing the 1978 May data set and a sixth-degree polynomial in analyzing the 1978 November–December data set.

The success of this method of absorbing noise by a polynomial is confirmed by the smallness of the postfit rms phase residuals (1.26 s for the 1978 May set, 0.60 s for the 1978 December set) compared to the estimated uncertainties in the observed pulse phase (1.34 s and 0.51 s respectively). If the residuals were independent, we could use the postfit rms error to determine the parameter uncertainties and obtain values close to those given as σ_o in Table 4. There is no guarantee, however, that the residuals are truly independent. They may still hide a term that varies on time scales close to the orbital period with an amplitude comparable to the rms of the residuals. In fact, we expect such a term due to the presence of red noise. Although small, this irreducible noise term nonetheless increases the parameter uncertainties by up to an order of magnitude (see the cols. labeled σ_t in Table 4). This effect is particularly noticeable where the quality of the data is high, as in the 1978 November–December data set.

c) *Best-Fit Orbital Parameters*

For each of the two data sets, we determined four orbital parameters in the manner discussed above: the local orbital epoch $T_{\pi/2}$, the projected semimajor axis $(a/c) \sin i$, the eccentricity e, and the longitude of periapsis ω. The best-fit values of these parameters were computed by iteration and were found to stabilize to within 0.01 σ after five iterations. The results are presented in Table 5. Two uncertainties are quoted for each parameter: a smaller one, which is that due to pulse-shape noise, and a larger one, which includes the uncertainty caused by fluctuations in rotation rate. These solutions

TABLE 4

EVALUATION OF THE OPTIMAL DEGREE FOR THE POLYNOMIAL INTRODUCED TO ABSORB THE RED NOISE IN ROTATION[a]

	Δa_1			Δb_1			Δa_2			Δb_2		
m[b]	σ_o	σ_r	σ_t	σ_o	σ_r	σ_t	σ_o	σ_r	σ_t	σ_o	σ_r	σ_t
1978 May												
1.....	0.25	1.14	1.16	0.44	2.55	2.58	0.37	1.14	1.19	0.28	1.45	1.48
2.....	0.25	1.10	1.13	0.44	1.41	1.48	0.37	0.49	0.61	0.28	0.36	0.46
3.....	0.26	0.64	0.69	0.45	0.67	0.81	0.37	0.40	0.54	0.28	0.23	0.37
4.....	0.26	0.66	0.71	0.45	0.70	0.84	0.37	0.35	0.51	0.28	0.16	0.33
5.....	0.27	0.58	0.64	0.45	0.68	0.82	0.38	0.26	0.46	0.28	0.16	0.33
6.....	0.29	0.60	0.66	0.48	0.60	0.77	0.38	0.23	0.44	0.29	0.17	0.33
7.....	0.29	0.63	0.70	0.48	0.69	0.84	0.38	0.21	0.43	0.29	0.15	0.32
8.....	0.30	0.60	0.67	0.49	0.65	0.82	0.38	0.20	0.43	0.29	0.15	0.33
9.....	0.36	0.58	0.69	0.57	0.58	0.81	0.40	0.15	0.42	0.29	0.15	0.33
1978 December												
1.....	0.069	2.93	2.93	0.136	3.55	3.55	0.145	5.11	5.11	0.074	0.82	0.82
2.....	0.071	1.41	1.41	0.137	3.41	3.41	0.148	1.38	1.39	0.074	0.80	0.81
3.....	0.073	0.86	0.86	0.141	1.81	1.82	0.149	1.19	1.20	0.075	0.67	0.67
4.....	0.075	0.95	0.95	0.142	1.58	1.59	0.152	0.31	0.35	0.075	0.70	0.71
5.....	0.075	0.94	0.95	0.159	1.06	1.07	0.152	0.29	0.32	0.081	0.38	0.39
6.....	0.083	0.83	0.83	0.162	0.81	0.83	0.152	0.28	0.32	0.083	0.27	0.28
7.....	0.117	0.84	0.85	0.172	0.89	0.90	0.153	0.28	0.32	0.084	0.27	0.28
8.....	0.143	0.73	0.74	0.191	0.82	0.85	0.153	0.28	0.32	0.086	0.26	0.27
9.....	0.416	0.68	0.80	0.193	0.82	0.84	0.157	0.28	0.32	0.096	0.26	0.27

[a] Δa_1, Δb_1, Δa_2, and Δb_2 are the orbital harmonic coefficients discussed in the text. σ_0, σ_r, and σ_t are the expected uncertainties (s) in each parameter due, respectively, to the short time scale fluctuations in pulse phase determined empirically from the local scatter (see Table 3), to the red noise in pulsar rotation with the strength given in the text, and to both sources of phase variation combined.

[b] Degree of the polynomial included in the fit.

TABLE 5

NEW ORBITAL SOLUTIONS FOR VELA X-1[a]

Data Set	Span (days)	N[b]	$T_{\pi/2}$[c] (JD 2,440,000+)	$(a/c)\sin i$ (s)	e	ω	m[d]	Satellite
1978 May	34	246	3651.536	112.6	0.090	151°	5	*OSO 8*
			(0.004)	(0.5)	(0.006)	(4)		
			(0.008)	(0.8)	(0.006)	(4)		
1978 Nov–Dec	37	269	3857.722	112.6	0.083	148	6	*HEAO 1*
			(0.001)	(0.2)	(0.002)	(2)		
			(0.011)	(0.8)	(0.006)	(4)		

[a] 1 σ single-parameter uncertainties are given in parentheses below the parameter values. The upper uncertainty includes only the uncertainty due to pulse-shape noise, while the lower uncertainty also includes that due to the red noise in rotation.

[b] Orbital cycle, counted from the time of mid-eclipse (JD 2,441,446.54) reported by Forman *et al.* 1973.

[c] Orbital epoch, defined as the time when the mean longitude equals $\pi/2$.

[d] Degree of local polynomial fit. $m = 5$ and $m = 6$ indicate that fifth- and sixth-degree polynomials, respectively, have been included in the fit in addition to the orbital parameters.

are stable against changes in the initial parameter values, and the parameter correlation coefficients are generally less than 0.5.

These results show that the uncertainty in the orbital parameters arising from the noise in the rotation of the neutron star is substantial. For the orbit derived from the *HEAO 1* data, for example, this noise increases the uncertainty in the semimajor axis and the local orbital epoch by factors of 4 and 10 respectively over the uncertainty due to the pulse-shape noise alone. Nevertheless, these are the most precise local solutions yet determined because of the size and quality of the data sets on which they are based. In the next section we combine them with other local solutions drawn from the literature to determine the most precise orbital elements that can be readily obtained from currently available data.

VI. MEAN ORBIT FOR VELA X-1

There are now some 20 published orbital solutions for Vela X-1 based on pulse-timing observations (see Table 6). It is therefore a useful undertaking to evaluate and combine these solutions to obtain an orbit having the smallest possible parameter uncertainties. As an explicit working definition, we suggest that a combined orbit should be based on at least two, and preferably more, independent local solutions of approximately equal weight, in order to provide adequate comparison. The solutions should also be well separated in time, in order to obtain meaningful information about secular changes in $P_{\rm orb}$ and ω. Each solution should have by itself adequate coverage in orbital phase to ensure that correlations between the parameter estimates are relatively small (less than 0.5 in magnitude). These criteria conform closely to the guidelines of Batten, Fletcher, and Mann (1978) for a definitive orbit based on spectroscopic radial velocities.

There is one essential difference between orbits based on pulse-timing observations and those based on spectroscopic data. In the case of a spectroscopic orbit, all radial velocity data can normally be combined into a single, global orbital solution. The analogous procedure is not generally applicable to pulse-timing observations because of the inherent noisiness of pulsar rotation. We discuss this point in more detail in § VII*b*, where we further justify the procedure of combining local solutions to produce a mean orbit. In the remainder of this section we describe specific criteria for incorporating individual solutions in the determination of our mean orbit for Vela X-1 and present the resulting orbital elements.

The 21 available orbital solutions are listed in Table 6. These include the two calculated in the present work and 19 previously published solutions. As mentioned in § V*a*, the highly uncertain time of periapsis reported by most previous authors has been converted to the more precise epoch in mean longitude by using the concurrently determined longitude of periapsis. The uncertainty in the epoch was estimated from the reported uncertainty in the projected semimajor axis, noting that these two parameters can be expressed as the coefficients of conjugate sinusoids in the solution and assuming that the observations provide uniform coverage of the orbit. Since the actual coverage is often quite nonuniform, this estimate of the uncertainty in the epoch could be in error by as much as a factor of 2.

In order to be included in the determination of our mean orbit, we required that a solution (1) be based solely on pulse-timing data, (2) include a full set of orbital elements, (3) be based on a block of data short enough to be covered by a single pulse ephemeris, and (4) have an eccentricity significant at the 3 σ level or better.

Ultimately, only five of the 21 solutions listed in Table 6 were selected for inclusion in the mean orbit. These chosen solutions are based on data obtained during 1975 June–July (Rappaport, Joss, and McClintock 1976); 1978 November (Rappaport, Joss, and Stothers 1980); 1978 May and 1978 December (this work); and 1980 March (Hayakawa 1981). Orbits published by van der Klis and Bonnet-Bidaud (1984) and by Nagase *et al.* (1984*b*) meet the above criteria but did not become available until after the completion of our analysis.

As discussed above, the presence of the random walk in pulse frequency (second-order red noise in pulse phase) intrinsic to the neutron star contributes to the uncertainty of the derived orbital parameters. In order to determine the appropriate weights to give the three previously published solutions in forming the combined solution, it was necessary to estimate the total uncertainty in the orbital parameters, including that due to noise in the rotation rate. However, this source of noise was not considered in any of the previously published solutions. Therefore, in addition to reconstructing the orbital epoch and its uncertainty, we have estimated the effect of the red noise on all the orbital parameters for these three solutions. The method used was the same as that for our two solutions (as discussed in § V), except that we did not have the liberty of altering the degree of the noise-absorbing polynomial included in the fit. The resulting parameter uncertainties are included in

TABLE 6

ORBITAL SOLUTIONS FOR VELA X-1[a]

Data Set	Span (d)	N[b]	$T_{\pi/2}$[bb] (244...)	O − C[c] (d)	$\frac{a}{c}\sin i$ (s)	e	ω (deg)	m[d]	Wt.	Ref.
1975 Feb...	9	112	2450.4[e]	+0.097	112	0.20	125	1	...	f
			(0.16)		(13)	(0.19)	(52)			
1975 Jun,	1	130	2611.71[g]	+0.048	111.4	0.126	146	1	1	h
Jul...	6		(0.015)		(1.7)	(0.021)	(12)			
			(0.087)		(3.7)	(0.040)	(26)			
1975 Nov...	18	143	(2728.43)[i]	(+0.230)	113.0	0.079[j]	162	2	...	k
			(0.02)		(2.4)	(0.009)	(15)			
1975 Nov...	19	143	2728.250	+0.050	113.0[kk]	0.116	166	2	...	l
			(0.007)		...	(0.008)	(3)			
1975 Dec,	10	...	(2750.0)[ll]	...	...	0.10	166	...	...	m
1976 May...	14		(2900.0)			(0.03)	(18)			
1976 Aug...	29	172	(2988.37)[i]	(+0.202)	112.5	0.073[j]	164	2	...	n
			(0.02)		(4.2)	(0.010)	(23)			
1976 Aug...	29	173	2997.128	−0.005	113.4	0.085	121	2	...	l
			(0.008)		(0.6)	(0.008)	(6)			
1978 May...	34	246	3651.536	0.000	112.6	0.090	151	5	36	This
			(0.004)		(0.5)	(0.006)	(4)			Paper
			(0.008)		(0.8)	(0.006)	(4)			
1978 May,	3	265	3821.81[e]	−0.050	114	0.10	150	1	...	o
Dec...	26		(0.02)		(1)	(0.01)	(9)	2		
1975 Jul,	6	265	3821.806[e]	−0.054	113.0	0.092	154	1	...	p
1978 Nov...	9		(0.010)		(0.8)	(0.005)	(5)	1		
1978 Nov...	9	265	3821.837[e]	−0.023	112.3	0.094	158	1	12	q
			(0.010)		(0.8)	(0.005)	(5)			
			(0.021)		(1.2)	(0.009)	(6)			
1978 Nov--	37	269	3857.722	+0.004	112.6	0.083	148	6	36	This
Dec...			(0.001)		(0.2)	(0.002)	(2)			Paper
			(0.011)		(0.8)	(0.006)	(4)			
1979 Mar...	14	278	3936.11[e,r]	(−2.288)	113.4	0.04	182	2	...	s
			(0.05)		(3.8)	(0.07)	(26)			
1979 Mar...	14	...	(3948.0)[t]	...	113.6	...	...	2	...	u
					(2.6)					
1979 Oct--	35	304	4171.437	−0.036	113.2	0.102	177	2	...	l
Nov...			(0.005)		(0.5)	(0.008)	(5)			
1980 Mar...	19	319	4305.937[e]	−0.003	114.4	0.091	160	2	...	s
			(0.018)		(1.3)	(0.019)	(7)			
1980 Mar...	19	319	4305.948[e]	+0.008	113.8	0.089	168	2	12	u
			(0.012)		(0.9)	(0.013)	(5)			
			(0.014)		(1.2)	(0.013)	(8)			
1979 Mar--	76	319	4305.944[e]	+0.004	113.9	0.079	155.3	2[v]	...	w
1981 Mar...			(0.008)		(0.6)	(0.007)	(2.5)			
1979 Mar--	114	399	5023.062[e]	−0.032	113.7	0.076	159	2[v]	...	x
1982 Mar...			(0.007)		(0.5)	(0.007)	(2.3)			
1979 Mar--	148	433	5327.874[e]	−0.011	114.1	0.080	157.3	2[v]	...	y
1982 Dec...			(0.007)		(0.5)	(0.006)	(2.1)			
1983 Mar...	15	442	5408.556[e]	−0.008	111.9	0.091	152	2	...	z
			(0.002)		(0.2)	(0.002)	(0.6)			

Table 6. As in Table 5, two uncertainties are quoted. The first is the uncertainty induced by pulse-shape noise alone, whereas the second includes our estimate of the uncertainty caused by the noise in rotation.

The uncertainty introduced by the noise in neutron star rotation is much less important for the three previously reported solutions than for the two solutions obtained in the present work, for two reasons. First, the count rates in the previous observations were much smaller than in the new observations reported here, with the result that the uncertainties due to photon statistics are much larger. Second, the data sets used in the previous solutions span smaller intervals, with the result that the expected excursion in pulse phase due to the noise in rotation is smaller.

We next determined the relative weights to be assigned to the locally determined parameters for the purpose of calculating the mean orbit. Minimum variance estimates for average parameters require that the weight assigned to each local parameter be proportional to its inverse variance. To follow this assignment rigorously would give each local solution a different weight for each parameter. For simplicity, each of the five local solutions was instead assigned a single weight, equal to the averaged formal weight of the four orbital parameters in each solution. The resulting relative weights are given in Table 6.

Using these weights, the semimajor axis and eccentricity of the mean orbit were calculated as averages of the corresponding local values reported for the five selected solutions. A central epoch and the orbital period were estimated by fitting a straight line to the five individual orbital epochs. The longitude of periapsis and its rate of change were similarly determined by fitting a straight line to the five individual longitudes.

Our mean orbit for Vela X-1 is recorded in Table 7. The quoted uncertainties are derived from the corresponding uncertainties in the parameter estimates of each of the five orbits, as described above, but they are also consistent with the scatter in these estimates among the five solutions used.

We also checked for a change in the orbital period by fitting a second-degree polynomial to the orbital epochs and found that the result was $\dot{P}_{\rm orb}/P_{\rm orb} = +2.7 \pm 2.6 \times 10^{-5}$ yr^{-1}. Since this value is consistent with zero $\dot{P}_{\rm orb}$, the quadratic fit to the orbital epochs is not given in Table 7. We adopt the value of $P_{\rm orb}$ derived from a linear fit to the orbital epochs as giving the best value of $P_{\rm orb}$ at the present time. The issue of apsidal advance in Vela X-1 is discussed elsewhere (Deeter *et al.* 1986*a*).

NOTES TO TABLE 6

[a] For ease in comparison, all errors have been converted to 1 σ single-parameter uncertainties. These uncertainties are listed in parentheses below the parameter estimates. For the five sets used in determining our mean orbit (Table 7), a second uncertainty is listed which takes into account the contribution from the red noise in pulsar rotation.

[b] Orbital cycle, counted from the time of mid-eclipse (JD 2,441,446.54) reported by Forman *et al.* 1973.

[bb] Orbital epoch, defined as the time when the mean longitude equals $\pi/2$.

[c] Residuals of the orbital epochs from the epoch ephemeris given by our mean orbit in Table 7.

[d] Degree of local polynomial fit. $m = 1$, linear fit for local period; $m = 2$, quadratic fit for local period and its derivative; $m = 5$ or 6, fifth- or sixth-degree polynomial included to absorb the red noise in rotation. Where two separate sets were fitted jointly, the degree used for each set is indicated. Where more than two separate sets were fitted jointly (i.e., for some of the *Hakucho* solutions), the indicated polynomial degree applies to all sets.

[e] Epoch inferred from T_ω and ω; error inferred from that given for $(a/c)\sin i$ (see text).

[f] *Copernicus* (Charles *et al.* 1978).

[g] Epoch inferred from $T'_{\pi/2}$ (time when the *true* longitude equals $\pi/2$), e, and ω; error in the epoch is one-fourth that in $T'_{\pi/2}$ (see DBP, Appendix A).

[h] *SAS 3* (Rappaport *et al.* 1976). Uncertainties were stated as 95% confidence limits and hence have been multiplied here by 0.5 to obtain 1 σ uncertainties.

[i] Estimated time of mideclipse ($T_{\rm mid}$) from eclipse observations. The orbital solution was constrained so that $T'_{\pi/2}$ (time when the true longitude equals $\pi/2$) agrees with this value.

[j] The uncertainty on this parameter is small by a factor of ~ 3 relative to the uncertainties on the other orbital parameters. Since this problem affects two data sets analyzed using the same program but reported separately, it is likely there is a minor bug in the program.

[k] *COS B* (Ögelman *et al.* 1977). Uncertainties were stated as 90% confidence limits and hence have been multiplied here by 0.6 to obtain 1 σ uncertainties.

[kk] $(a/c)\sin i$ was set equal to the value obtained in the earlier solution by Ögelman *et al.* 1977.

[l] *COS B* (van der Klis and Bonnet-Bidaud 1984). The 1975 Nov and 1976 Aug are second-pass solutions to those reported earlier by Ögelman *et al.* 1977 and Molteni *et al.* 1982. Uncertainties were stated as 1 σ multiparameter errors and hence have been multiplied by 0.35 to convert them to 1 σ single-parameter errors.

[ll] Values for the orbital epoch and $(a/c)\sin i$ were not reported for either of these data sets. The listed times may be taken as approximate epochs for these sets, and an average of them as an epoch for e and ω.

[m] *OSO 8* (Becker *et al.* 1978). Uncertainties were stated as 90% confidence limits and hence have been multiplied here by 0.6 to obtain 1 σ uncertainties.

[n] *COS B* (Molteni *et al.* 1982). The confidence level for the uncertainties was not clearly stated, but since the program used to obtain the parameters was the same used by Ögelman *et al.* 1977 for the 1975 Nov set, it is likely that they are also 90% confidence limits. Therefore, the uncertainties have been multiplied here by 0.6 to convert them to 1 σ limits.

[o] *HEAO 1* A-4 (Bautz *et al.* 1983).

[p] SAS *3* (Rappaport *et al.* 1980). This is a joint solution combining the 1975 Jul and 1978 Nov sets. Two additional parameters were determined in this solution: $P_{\rm orb} = 8.9649 \pm 0.0002$ days, and $\dot{\omega} = +0\overset{\circ}{.}4 \pm 1\overset{\circ}{.}7$ yr^{-1}. The epoch for $\dot{\omega}$ is not clearly stated. In the absence of any other indication, we have assumed that the epoch is identical to the given time of periapsis (JD 2,443,823.40).

[q] *SAS 3* (Rappaport *et al.* 1980).

[r] Either the given T_ω (JD 2,443,938.4) or ω is incorrect. The inferred $T_{\pi/2}$ should agree much more closely with the orbital ephemeris. If the given epoch is really $T_{\pi/2}$, then $O - C = +0.002$ days, which is much more satisfactory.

[s] *Hakucho* (Nagase *et al.* 1981).

[t] No orbital epoch was given for this solution. The indicated time is approximately the midtime of the data interval and may be taken as the epoch for $(a/c)\sin i$.

[u] *Hakucho* (Hayakawa 1981). These are apparently "second-pass" solutions, using essentially the data reported by Nagase *et al.* 1981. The 1979 Mar solution was for a circular orbit, so e and ω were not reported.

[v] All sets included in the joint fit were fitted by a quadratic (second-degree) polynomial.

[w] *Hakucho* (Nagase 1981). Joint fit to seven separate sets of data. The orbital period was not determined in this solution, but was fixed at 8.9641 days as determined from the eclipses.

[x] *Hakucho* (Nagase *et al.* 1982). Joint fit to 11 separate sets of data. The orbital period was determined to be $P_{\rm orb} = 8.9641 \pm 0.0002$ days.

[y] *Hakucho* (Nagase *et al.* 1984*a*). Joint fit to 14 separate sets of data, including those used in the preceding listing. The orbital period and the rate of apsidal advance were determined to be $P_{\rm orb} = 8.9641 \pm 0.0006$ days and $\dot{\omega} = +0\overset{\circ}{.}3 \pm 1\overset{\circ}{.}1$ yr^{-1}.

[z] *Tenma* (Nagase *et al.* 1984*b*).

TABLE 7

MEAN ORBITAL PARAMETERS FOR VELA X-1

Parameter[a]	Value[b]
$T_{\pi/2}$	2,443,821.8604 ± 0.0056 HJD
P_{orb}	8.96443 ± 0.00022 days
$(a/c) \sin i$	112.70 ± 0.47 s
e	0.0881 ± 0.0036
ω	152°.8 ± 2°.2[c]
$\dot{\omega}$	+6°.9 ± 3°.4 yr^{-1}
$f(M)$[d]	19.12 ± 0.24 $M_\odot$

[a] $T_{\pi/2}$ is the orbital epoch, defined as the time when the mean longitude equals $\pi/2$. All other symbols have their usual meanings. For a discussion of this choice of orbital parameters, see DBP.

[b] Indicated errors are 1 σ single-parameter uncertainties.

[c] At the epoch $T_{\pi/2}$ listed.

[d] Derived parameter.

VII. DISCUSSION

With the experience gained in the present study, we are able to place in a general context the problem of determining the orbit of a binary pulsar in the face of red noise and to advocate a particular approach in determining and presenting orbital solutions. In the present section we discuss the conditions under which red noise in pulse phase has an important effect on the estimation of orbital parameters, evaluate three approaches to obtaining orbital solutions, and discuss the implications of our results for the design of pulse timing experiments.

a) Effects of Noise

The uncertainties in the parameters of an orbital solution are due to noise in the measured pulse phase. In the present context, there are two major sources of noise: (1) fluctuations in the rotation rate of the star and (2) fluctuations in the observed pulse shape. In Vela X-1 there is a component in the observed power spectrum of the noise in pulse phase that varies with analysis frequency roughly as f^{-4} (Paper II). This spectrum is consistent with random-walk fluctuations in the rotation rate of the neutron star. As for the fluctuations in the observed pulse shape, there are two contributions. One arises from the discrete nature of the photon emission process and leads to white noise in the measured pulse phase. The strength of this noise depends on the number of photons detected and therefore on the properties of the measuring apparatus as well as on those of the source. The second contribution is any fluctuation in pulse shape in *excess* of that due to photon statistics. Such excess shape fluctuations have been measured in Her X-1 (Boynton and Deeter 1979) as well as in Vela X-1 (§ IV above). In both sources, the excess shape fluctuations are *observed* to produce white noise in the measured pulse phase, at least on time scales longer than a few pulse periods (Paper II). Thus, the total noise in phase produced by both contributions to shape fluctuations is also white and therefore induces a component in the power spectrum of noise in pulse phase that is independent of analysis frequency (f^0 power law).[7]

[7] Our division of the noise in pulse phase into two classes, arising from noise in pulse shape and noise in rotation rate, is based on the presence of two distinct components in the power spectrum of the noise in pulse phase. Furthermore, for the present data on Vela X-1, the measured shape fluctuations completely account for the observed strength of the white noise component in the power spectrum (Paper II). Thus, any white noise in pulse phase contributed by fluctuations in the rotation rate of the star is small.

From this description it is apparent that the power density of the red noise in pulse phase must equal the power density of the white noise at some *crossover frequency* f_c (Lamb 1979; Boynton and Deeter 1979). Adopting consistent units for the strength of the random walk in the rotation S_{rot} (rad^2 s^{-3}) and the strength of the combined white noise processes, S'_{white} (rad^2 s), this crossover frequency is given by

$$f_c = \frac{1}{2\pi}\left(\frac{S_{rot}}{S'_{white}}\right)^{1/4} . \quad (12)$$

Below f_c, the red noise dominates the total power density; above it, the white noise dominates. Here and in the following, we use primes to distinguish strengths that depend on experimental parameters from those that depend only on source properties. For the purpose of estimating orbital parameters or investigating the character of fluctuations in neutron star rotation, the largest possible crossover frequency is generally desirable. It is therefore useful to see how S'_{white} can be minimized through the design of the timing experiment.

According to the previous discussion, the total white noise strength can be written as the sum of two components, $S'_{white} = S'_{phot} + S'_{excess}$. We can easily adapt equation (6) to specify S'_{phot} as a noise power per unit bandwidth (Deeter 1984), noting that for Poisson statistics the mean count rate is given by $a = A\Phi$ and its variance by $\sigma_a^2 = \alpha/\beta T$, so that $\sigma_a^2/a^2 = 1/A\Phi\beta T$, and

$$S'_{phot} = \frac{\sigma_\tau^2}{T^{-1}} = \frac{1}{\beta A \Phi P^{-1}\int_0^P [g'(\phi)]^2 d\phi} = \frac{1}{\beta A} s_{phot} . \quad (13)$$

Here β is the ratio of the detector "live" time to the total time span T of the data set, A is the effective area of the detector, and Φ is the incident X-ray photon flux. To demonstrate the scaling of S'_{phot} with the design parameters β and A, we have written S'_{phot} as the product of $1/\beta A$ and a remaining factor s_{phot} that depends only on source properties.

For pulse timing with unfiltered pulses, an expression for S'_{excess} also follows from equation (6) but with the condition that the fractional variance σ_a^2/a^2 is independent of the mean counting rate and therefore independent of detector area. However, this variance does depend inversely on the *number* of independent pulses observed. Consequently, we define the parameter γ as the ratio of the number of pulses incorporated in all the folded masters to the total number of pulses emitted in the time span of the recorded data,[8] and repeat the argument leading to equation (13) to obtain $S'_{excess} = (1/\gamma)S_{excess}$. S_{excess} is the noise strength for the ideal situation of complete sampling of the pulses and does *not* depend on experimental parameters such as the detector area. Combining this result with equation (13), we may write

$$S'_{white} = \frac{1}{\beta A} s_{phot} + \frac{1}{\gamma} S_{excess} . \quad (14)$$

This equation indicates that higher sampling density (larger β and γ) necessarily reduces S'_{white} and increases f_c, whereas increased detector area cannot increase f_c after S'_{phot} is reduced much below S'_{excess}.

The relative contributions of S'_{phot} and S'_{excess} depend on the ratio $\beta A/\gamma$. This ratio is considerably smaller for the *OSO 8*

[8] There is a subtle distinction between β and γ in that $1-\beta$ incorporates *all* sources of detector "dead" time, while $1-\gamma$ accounts only for dead time that reduces the number of independent pulses. For example, β is sensitive to data gaps on time scales shorter than the pulse period, while γ is not.

experiment than for the *HEAO 1* experiment. Thus, even though the pulse shape fluctuations due to photon-counting noise were comparable to those due to excess shape noise in the *OSO 8* data, they were negligible in the *HEAO 1* data. The strength of the white noise in phase was further reduced in the *HEAO 1* data by filtering the pulse waveforms. As a result, the crossover frequency for the *HEAO 1* experiment is ~ 2.5 times higher than that for the *OSO 8* experiment.

The red noise in pulse phase affects the parameters of an orbital solution if the span T of data analyzed is longer than f_c^{-1}. Typically, the least-squares fitting problem is well posed only if the data span is at least one orbit. Thus, loosely speaking, the effect of the red noise must be taken into account if it dominates for data spans equal to the orbital period, or equivalently, if the crossover frequency is comparable to or greater than the orbital frequency. As we have shown, longer spans may be analyzed by controlling the low-frequency leakage of red noise power into the parameter estimates with a noise-absorbing polynomial. However, the polynomial degree m must be no more than twice the number of orbits in the data span, i.e., one must have $m \leq 2f_{\rm orb} T$; otherwise the polynomial will interfere with the orbital function, increasing the parameter variances and covariances.

For the *OSO 8* experiment, the observed crossover frequency is $\sim$(8 days)$^{-1}$, while for the *HEAO 1* experiment it is only (3 days)$^{-1}$. Because the data from both experiments span roughly 35 days, one would not expect to be able to neglect the effect of the red noise in analyzing either one. For the *HEAO 1* experiment, in particular, the red noise increased the uncertainties in the orbital parameters by roughly an order of magnitude over the uncertainties due to pulse shape fluctuations alone (see Table 4).

b) *Approaches to Determining the Orbit*

Historically, there have been three different approaches to determining orbital elements by pulse-timing techniques. In the *global* approach, a single function consisting of orbital terms plus a polynomial is fitted to the entire span of data. In the *local* approach, the data are partitioned into suitable blocks and a function consisting of orbital terms plus a polynomial is fitted to each block; the orbital parameters derived from the different blocks are then averaged to produce the final estimates. Some authors have adopted a *hybrid* approach, in which the data are partitioned into separate blocks but all blocks are fitted simultaneously; this is done by including a separate polynomial for each block together with a single orbital function for the entire span of data. Here we argue that if red noise is present, a suitably constructed local approach has greatest utility without sacrificing precision.

The global approach is certainly appropriate in the absence of red noise, since the rotation history can then be globally modeled by a low-degree polynomial (to account for secular variation). Such is the case for the binary pulsar 1913 − 16, for which a 6.5 yr data span is well fitted by an orbit plus cubic polynomial (Taylor and Weisberg 1982). However, in the presence of substantial red noise a high-degree polynomial might be required. For comparison, if *HEAO 1* observations uniformly sampling Vela X-1 were available over a 6.5 yr span, a polynomial of degree 500 would be necessary to absorb adequately the red noise. Even so, the global approach is generally not possible for accretion-powered pulsars, since the observing intervals are separated by gaps of sufficient length and the red noise is of sufficient strength that a correct pulse count cannot be maintained across the gaps.

The presence of gaps in the data is one of the primary motivations for employing either the local or hybrid approach. The hybrid method provides some reduction in the number of free parameters relative to the global approach, but at the cost of introducing substantial complexity into the problem of propagating the red noise into the parameter estimates.

Even without gaps in the data, the local approach is natural for sources that exhibit red noise, because the ever-increasing nondeterministic phase shift that accumulates between a given pulse and later pulses tends to "decouple" the phases of widely separated pulses. This suggests that no more information is contained in a long stretch of data than can be extracted by a series of local fits. The blocks into which the complete data set is divided do not necessarily have to be small enough that the red noise can be neglected but only small enough that it can be adequately absorbed by including a polynomial of relatively low degree in the fit. On the other hand, the blocks should span substantially more than a single orbital cycle with fairly uniform coverage in orbital phase in order to avoid large correlations between the orbital parameters. The uncertainties in the parameters and the correlations between them can then be estimated correctly, using the method outlined in the Appendix.

In the present work we chose to treat the new data as two four-orbit blocks. The polynomials required to absorb the red noise over four orbits were of fifth and sixth degree, the regression problem was well posed, and the correlations between orbital elements were well controlled (correlation coefficients less than 0.5).

In addition to yielding a regression problem with a small number of parameters and consequently a relatively simple error propagation procedure, the local approach has two other advantages over the global and hybrid methods. First, construction of an overall solution by averaging a set of local solutions makes possible a check on the reliability of the component solutions by comparing them with one another. Second, the information provided by future observations of a given source can be easily combined with the information extracted from earlier observations to yield a refined solution without reanalyzing any of the earlier data.

As an example of the second advantage of the local approach, we note that the orbital period, as well as slowly varying parameters such as the rate of change of the orbital period and the rate of apsidal advance, need not be included in the local solutions. Instead, the orbital period and its rate of change can be determined by a subsequent fit to a set of locally determined epochs in mean longitude, while the apsidal advance rate can be determined from a set of longitudes of periapsis (see Deeter *et al.* 1986*a*).

Because of its many advantages, we advocate adoption of the local approach in analyzing future observations of Vela X-1 and other accretion-powered pulsars that exhibit red noise in pulse phase.

c) *Implications*

We now consider the implications of these results for the design of pulse-timing experiments, including both the properties of the apparatus and the data sampling structure. The crossover frequency f_c defined by equation (12) is a rough measure of the quality of data for study of the properties of the red noise component. Reducing the strength of the white noise

component improves pulse-timing precision and increases the crossover frequency, making possible study of the properties of the red noise component at higher frequencies. This can be done by increasing the fractional "live" time of the detector (in the sense of increasing β and γ in eq. [14]). The part of the white noise component that is due to photon noise can also be reduced by increasing the effective detector area. However, once the detector area is large enough that excess shape noise dominates, a further increase does not improve the quality of the data for the study of the red noise, since the contribution from excess shape noise is independent of the detector area. Increasing the detector area may still be crucial for study of the pulse-shape fluctuations themselves.

Taken at face value, this excess noise in pulse shape appears to limit the improvement in pulse-timing precision that could be achieved by increasing the detector area. For Vela X-1, this limitation is already apparent in the *HEAO 1* experiment discussed here—the noise in pulse phase induced by excess shape noise dominates the noise induced by photon statistics by a factor of roughly 30. However, we have shown that the white noise component arising from excess shape noise *can* be reduced by appropriate treatment of the data before the pulse-phase time series is constructed. For example, the simple filtering procedure used here reduced the contribution made by excess shape noise by a factor of almost 4 for the *HEAO 1* data. Stated differently, the effective area of this experiment was increased by nearly a factor of 4 by using this technique. A more general filtering method has now been developed that may reduce the deleterious effects of excess shape noise still further (Boynton and Deeter 1985). A better understanding of the excess pulse shape fluctuations may well make possible the development of still more powerful techniques to reduce their contribution to the uncertainty in pulse phase.

Our results indicate that a quantitative survey of the character of excess shape noise in accretion-powered pulsars is essential for planning future observations. One reason is that optimal use of large-area detectors for pulse-timing studies requires knowledge of both the pulse shape and the spectrum of excess shape noise in candidate sources. Second, this same information is needed to evaluate the promise of a given pulsar as a probe of neutron star structure and accretion physics. Third, optimal allocation of limited observing resources between candidates also depends on the character of the excess pulse-shape noise. Finally, such a survey augmented with provisional knowledge of the noise in rotation is necessary in order to select the appropriate time scales for a detailed study of the noise in the rotation rate of a given pulsar.

VIII. CONCLUSION

In the present paper we have redetermined the orbit of Vela X-1 from new data. By combining our solutions with other, published solutions, we have constructed a mean orbit of improved precision. During the course of this study we have developed a procedure to estimate the uncertainty in the orbital elements induced by the red noise in pulse phase that is present in this source. This procedure may be used to estimate the uncertainties in the orbits of other pulsars that exhibit red noise. We emphasize that although our method provides a rigorous treatment of the uncertainty due to the simultaneous presence of both red and white noise in pulse phase, it does not necessarily lead to the minimum possible uncertainty in the orbital parameters. Thus, it may be possible to further reduce this uncertainty if a more refined method is developed.

This is the first work to consider the uncertainty in the orbital elements induced by the red noise in pulse phase, which dominates all other sources of uncertainty by about an order of magnitude for the highest quality data that we analyzed. Nevertheless, the orbital elements reported here are the most precise reported to date, because the solution is based on a large quantity of high–count-rate data.

We have argued strongly for adoption of a local approach to determining the orbits of accretion-powered pulsars. This approach has many advantages over other methods that have been used in the past, including numerical tractability, a simple error propagation procedure, an internal check on the reliability of the solution, and ease of successive refinement of the orbital solution as more data are accumulated.

Although we have encountered a significant limitation to pulse-timing precision imposed by fluctuations in pulse shape in excess of those due to photon count statistics, we have developed a simple method of filtering the pulse waveform that substantially improves precision in measuring pulse phase, reducing this limitation. The same method can also be applied to other pulsars that exhibit excess fluctuations in pulse shape. Without some filtering technique, no increase in detector area will significantly improve the precision of pulse timing when excess shape noise is dominant. The development of still more powerful analysis techniques is crucial to achieve precision in pulse timing that may otherwise be beyond reach. The study of pulse-shape variability is also clearly important for increasing our understanding of pulsar physics, as well as for improving pulse-timing capabilities.

In the second paper of this series (Deeter *et al.* 1986*b*) we describe the construction of a pulse-frequency record for Vela X-1, the computation of a low-resolution power density spectrum of the fluctuations in the star's angular acceleration, and the key elements of the experimental design. The question of apsidal advance in Vela X-1 and the implications of the Vela X-1 frequency record and power density spectrum for neutron star structure and accretion physics will be addressed in separate publications (Deeter *et al.* 1986*b*; Lamb *et al.* 1986).

It is a pleasure to thank S. Pravdo, N. White, K. Wood, and D. Yentis for their assistance in planning and carrying out this series of *HEAO 1* pointings. We also thank the *OSO 8* group and especially P. Serlemitsos for providing unpublished *OSO 8* data for use in this study. We are grateful to the *SAS 3* group and especially H. Bradt for arranging the special 1979 January *SAS 3* observation and for assembling the data from this observation. We thank D. Pakey for help in assembling the *HEAO 1* A-1 data and D. Percival for assistance in the early stages of the data analysis. Finally, we are grateful to the Aspen Center for Physics for their warm hospitality during the Pulsar Workshop in 1984 August. F. K. L. wishes to thank V. Petrosian, P. Sturrock, and R. Wagoner for their kind hospitality at Stanford University and the John Simon Guggenheim Memorial Foundation for its generous support. This research was supported in part by NSF grants AST 80-01471 and AST 82-16661 (at Washington), PHY 78-04404 and PHY 80-25605 (at Illinois), and PHY 81-18387 (at Stanford); and by NASA grants NAS 8-33360 (at Washington), NSG 7653 (at Illinois), and NGR 05-020668 (at Stanford).

APPENDIX

ERROR ANALYSIS FOR PARAMETER ESTIMATES USING SAMPLING FUNCTIONS

In the body of this paper we confront the problem of determining orbital parameters from a time series containing red noise. Our approach is to use the ordinary least-squares technique, assuming uncorrelated errors in the data and including a polynomial of moderate degree to approximately model or "absorb" the red noise. As part of this scheme, we choose the polynomial degree to make the parameter uncertainties as small as possible. In order to carry out the scheme, we must be able to compute parameter uncertainties which take into account the presence of residual red noise not absorbed by the polynomial.

Unfortunately, the parameter uncertainties provided by the least-squares solution describe only the *uncorrelated* errors in the data and therefore do not include the errors contributed by the red noise. Nevertheless, the contribution to parameter uncertainties made by correlated noise (including red noise of any order) *can* be calculated through an error propagation analysis. In this approach, each parameter is written in terms of a sampling function applied to the data, where the sampling function is specified by the solution to the least-squares problem. Using this sampling function formalism (Deeter 1984), we can compute the expected uncertainty in each parameter due to the presence of red noise in the data. This Appendix deals with the algebraic manipulations required to reach this goal.

In a linear problem the observations x_i are connected to the parameters y_j through the equations of condition:

$$x_i = \sum_j y_j g_{ji} \,. \tag{A1}$$

For this to be a well-posed problem, the parameters must be overconstrained; that is, there must be more observations than parameters. In some cases, the parameters can be regarded as coefficients on specified functions $g_j(t)$, which are sampled at discrete points t_i in time. The equations of condition can then be written

$$x(t_i) = \sum_j y_j g_j(t_i) \,. \tag{A2}$$

The ordinary least-squares solution using identical point weights is obtained by inverting the normal equations, written in matrix form as $\boldsymbol{A}\boldsymbol{y} = \boldsymbol{b}$, wherein

$$A_{jk} = \sum_i g_{ji} g_{ki} \,, \quad b_j = \sum_i g_{ji} x_i \,, \tag{A3}$$

and $\boldsymbol{y}$ is the vector of parameters. This solution minimizes the sum of squares of observational residuals, and when the observations have equal and uncorrelated errors this solution gives unbiased, minimum-error parameter estimates. For errors of this type, the parameter covariance matrix is given by the inverse of the matrix $\boldsymbol{A}$, that is,

$$\text{cov}\,(y_j, y_k) = (\boldsymbol{A}^{-1})_{jk} \sigma^2 \,, \tag{A4}$$

where σ^2 is the common observational variance.

For other types of errors in the observations, this solution is not necessarily optimal (i.e., the parameter estimates may not have minimum errors). However, the optimal solution can sometimes be obtained by modifying the normal equations. For example, in the case of unequal but uncorrelated errors, use of point weights proportional to the inverse variances instead of equal weights gives the optimal solution. In the more general case of correlated errors, a weight matrix obtained as the inverse of the data covariance matrix has to be used. The optimal solution for this case can still be expressed in terms of normal equations, but the algebra is more complicated.

The case of data containing red noise presents an even more difficult situation, since the uncertainties in the observations no longer exhibit a true covariance matrix, although a quasi-covariance matrix may be defined for red noise, as discussed below. Unfortunately, this quasi-covariance matrix is not positive definite, and therefore cannot be used in the same way as a true covariance matrix for generating a data weight matrix. An alternative approach (until a mathematically more rigorous approach is found) is to absorb the red noise into polynomial terms, introducing enough terms to reduce the residuals to approximately the size expected from uncorrelated observational errors. The utility of this method stems from the fact that it can be used to propagate the red noise into parameter errors, even though white noise was assumed in generating the weight matrix.

In order to simplify our exposition, we assume that the observational noise consists of equal, uncorrelated errors. We assume that red noise with known properties is also present. By inverting the normal equations, the parameters y_j can be expressed in terms of the observations x_i:

$$y_j = \sum_k (\boldsymbol{A}^{-1})_{jk} \sum_i g_{kl} x_i = \sum_i \hat{g}_{ji} x_i \,. \tag{A5}$$

In the last expression on the right, the substitution $\hat{g}_{ji} = \sum_k (\boldsymbol{A}^{-1})_{jk} g_{ki}$ has been made. In the interpretation of the least-squares problem as determining coefficients on functions, we may write $\hat{g}_j(t_i) = \hat{g}_{ji}$. The functions $\hat{g}_j$ may then be regarded as sampling functions applied to the observed data, having the additional property that they produce parameter estimates. The two sets of functions $g_j(t)$ and $\hat{g}_j(t)$ are dual in the sense that they satisfy a cross-orthonormality condition, namely,

$$\sum_i g_{ji} \hat{g}_{ki} = \delta_{jk} \,. \tag{A6}$$

This result will be used shortly.

The interpretation of the solution to the least-squares problem as a set of sampling functions applied to the data allows *any* observational noise possessing a true covariance matrix to be propagated into parameter uncertainties. The parameter covariance matrix is given by the expression

$$\text{cov}\,(y_j, y_k) = \sum_i \sum_l \hat{g}_{ji}\hat{g}_{kl}\,\text{cov}\,(x_i, x_l)\,. \tag{A7}$$

For the assumed observational noise, which has equal and uncorrelated errors, the parameter covariance matrix reduces to the inverse of the normal equations

$$\text{cov}\,(y_i, y_k) = \sum_i \hat{g}_{ji}\hat{g}_{ki}\sigma^2 = (A^{-1})_{jk}\sigma^2\,. \tag{A8}$$

For the case of rth-order red noise, the parameter covariance matrix is given by another simple formula, namely,

$$\text{cov}_r\,(y_j, y_k) = \frac{(-1)^r}{2(2r-1)!}\,S_r \sum_i \sum_l \hat{g}_{ji}\hat{g}_{kl}\,|t_i - t_l|^{2r-1}\,, \tag{A9}$$

where S_r is the strength of the noise (see Deeter 1984, Appendix). It should be noted that equation (A9) is valid only for those "functions" $\hat{g}_j$ that satisfy the moment conditions

$$\sum_i \hat{g}_j(t_i)t_i^k = 0\,, \qquad 0 \le k < r\,. \tag{A10}$$

If polynomials up to degree $r-1$ are included among the functions g_j (whose coefficients are being estimated), the dual function corresponding to any other of the functions included in the fit will satisfy the moment conditions by the cross-orthonormality relationships (eq. [A6]). The resulting parameter covariance matrix is then valid for the remaining coefficients.

It should now be clear what is meant by a "quasi-covariance" matrix for the red noise process. A comparision of the parameter covariance matrix for red noise (eq. [A9]) with the general expression for observational noise possessing a true covariance matrix (eq. [A7]) suggests the definition

$$C_{il} \equiv \text{cov}_r\,(x_i, x_l) \equiv \frac{(-1)^r}{2(2r-1)!}\,|t_i - t_l|^{2r-1}S_r\,. \tag{A11}$$

We emphasize again that C is *not* a true covariance matrix, since the diagonal terms are zero whereas the off-diagonal terms grow with the time difference. This behavior is in marked contrast to the behavior of a "normal" covariance matrix, which has positive diagonal terms and off-diagonal terms that generally decrease with the time difference. Indeed, this matrix is not positive definite, unlike a normal covariance matrix. However, these properties in no way reduce the utility of equation (A9) for computing the correct parameter variances and covariances for red noise.

The approach of this Appendix provides a rigorous treatment of *error propagation* (that is, the problem of determining the effect of a given noise process on the uncertainty of a parameter) in the presence of power-law red noise. It does *not* provide a rigorous approach to the problem of *minimizing the parameter errors* in the face of such noise. Solving this latter problem requires that the properties of the noise in the data be correctly taken into account when setting up the least-squares equations, rather than the ad hoc approach of "absorbing" red noise by polynomial terms. As is the case with any least-squares solution, the parameter errors would then be available as a natural part of the solution (i.e., the inverse of the matrix of normal equations). In this more general approach, one can still use the error propagation through sampling functions to compute the parameter errors, but the errors derived this way serve only as a check on the errors supplied by the least-squares solution. The possibility of a rigorous approach to the problem of minimizing the parameter errors became apparent only after we had completed the analysis presented in this paper, and we intend to investigate this topic further.

REFERENCES

Batten, A. H., Fletcher, J. M., and Mann, P. J. 1978, *Pub. Dominion Ap. Obs.*, **15**, 121.
Bautz, M., Howe, S., Gorecki, A., Lang, F., Levine, A., Primini, F., and Lewin, W. H. G. 1983, *Ap. J.*, **266**, 794.
Becker, R. H., Rothschild, R. E., Boldt, E. A., Holt, S. S., Pravdo, S. H., Serlemitsos, P. J., and Swank, J. H. 1978, *Ap. J.*, **221**, 912.
Boynton, P. E. 1981, in *IAU Symposium 95, Pulsars*, ed. W. Sieber and R. Wielebinski (Dordrecht: Reidel), p. 279.
Boynton, P. E., and Deeter, J. E. 1979, in *Compact Galactic X-ray Sources*, ed. F. K. Lamb and D. Pines (Urbana: University of Illinois at Urbana-Champaign, Phys. Dept.), p. 168.
———. 1985, in *Proc. Inuyama Workshop on Timing Studies of X-Ray Sources*, ed. S. Hayakawa and F. Nagase (Nagoya University, Dept. of Ap.), p. 13.
Boynton, P. E., Deeter, J. E., Lamb, F. K., Zylstra, G., Pravdo, S. H., White, N. E., Wood, K. S., and Yentis, D. J. 1984, *Ap. J. (Letters)*, **283**, L53.
Buff, J., *et al.* 1977, *Ap. J.*, **212**, 768.
Charles, P. A., Mason, K. O., White, N. E., Culhane, J. L., Sanford, P. W., and Moffat, A. F. J. 1978, *M.N.R.A.S.*, **183**, 813.
Chubb, T. A. 1976, in *Pittsburgh Conference on BL Lac Objects*, ed. A. M. Wolfe (Pittsburgh: University of Pittsburgh, Dept. of Phys. and Astr.), p. 163.
Cordes, J. M., and Helfand, D. J. 1980, *Ap. J.*, **239**, 640.
Deeter, J. E. 1984, *Ap. J.*, **281**, 482.
Deeter, J. E., and Boynton, P. E. 1982, *Ap. J.*, **261**, 337.
———. 1985, in *Proc. Inuyama Workshop on Timing Studies of X-Ray Sources*, ed. S. Hayakawa and F. Nagase (Nagoya University, Dept. of Ap.), p. 29 (DB).
Deeter, J. E., Boynton, P. E., Lamb, F. K., and Zylstra, G. 1986*a*, *Ap. J.*, submitted.
———. 1986*b*, preprint (Paper II).
Deeter, J. E., Boynton, P. E., and Pravdo, S. H. 1981, *Ap. J.*, **247**, 1003 (DBP).
Deeter, J. E., Boynton, P. E., Shibazaki, N., Lamb, F. K., Hayakawa, S., Nagase, F., and Sato, N. 1986*c*, in preparation.
Downs, G. S., and Reichley, P. E. 1983, *Ap. J. Suppl.*, **53**, 169.
Dupree, A. K., *et al.* 1980, *Ap. J.*, **238**, 969.
Elsner, R. F., and Lamb, F. K. 1976, *Nature*, **262**, 256.
———. 1977, *Ap. J.*, **215**, 897.
Epstein, R. 1977, *Ap. J.*, **216**, 92.
Forman, W., Jones, C., Tananbaum, H., Gurksy, H., Kellogg, E., and Giacconi, R. 1973, *Ap. J. (Letters)*, **182**, L103.
Groth, E. J. 1975, *Ap. J. Suppl.*, **29**, 443.
Hayakawa, S. 1981, *Space Sci. Rev.*, **29**, 221.

Henrichs, H. F. 1983, in *Accretion-driven Stellar X-ray Sources*, ed. W. H. G. Lewin and E. P. J. van den Heuvel (Cambridge: Cambridge University Press), p. 393.
Inoue, H. 1984, in *High Energy Transients in Astrophysics*, ed. S. E. Woosley (New York: AIP Conf. Proc., No. 115), p. 243.
Kallman, T. K., and White, N. E. 1982, *Ap. J.* (*Letters*), **261**, L35.
Lamb, F. K. 1977, in *Proc. 8th Texas Symposium on Relativistic Astrophysics* (*Ann. NY Acad. Sci.*, **302**), p. 482.
———. 1979, in *Compact Galactic X-Ray Sources*, ed. F. K. Lamb and D. Pines (Urbana: University of Illinois at Urbana-Champaign, Phys. Dept.), p. 143.
Lamb, F. K., Pethick, C. J., and Pines, D. 1973, *Ap. J.*, **184**, 271.
Lamb, F. K., Zylstra, G., Boynton, P. E., and Deeter, J. E. 1986, in preparation.
McClintock, J. E., *et al.* 1976, *Ap. J.* (*Letters*), **206**, L99.
Molteni, D., Rapisarda, M., Re, S., and Robba, N. R. 1982, *Astr. Ap.*, **111**, 365.
Nagase, F. 1981, *Space Sci. Rev.*, **30**, 395.
Nagase, F., *et al.* 1981, *Nature*, **290**, 572.
Nagase, F., *et al.* 1982, *ISAS Research Note*, No. 178.
Nagase, F., *et al.* 1984*a*, *Ap. J.*, **280**, 259.
Nagase, F., *et al.* 1984*b*, *Pub. Astr. Soc. Japan*, **36**, 667.
Ögelman, H., Beuermann, K. P., Kanbach, G., Mayer-Hasselwander, H. A., Capozzi, D., Fiordilino, E., and Molteni, D. 1977, *Astr. Ap.*, **58**, 385.
Pringle, J. E., and Rees, M. J. 1972, *Astr. Ap.*, **21**, 1.
Rappaport, S., Joss, P. C., and McClintock, J. E. 1976, *Ap. J.*, (*Letters*), **206**, L103.
Rappaport, S., Joss, P. C., and Stothers, R. 1980, *Ap. J.*, **235**, 570.
Rothschild, R. *et al.* 1979, *Space Sci. Instr.*, **4**, 269.
Serlemitsos, P. J., Becker, R., Boldt, E. A., Holt, S. S., Pravdo, S., Rothschild, R., and Swank, J. H. 1976, in *X-ray Binaries*, *Proc. Goddard Conference*, ed. E. Boldt and Y. Kondo (NASA SP-389), p. 67.
Staubert, R., Kendziorra, E., Pietsch, W., Reppin, C., Trümper, J., and Voges, W. 1980, *Ap. J.*, **239**, 1010.
Taylor, J. H., and Weisberg, J. M. 1982, *Ap. J.*, **253**, 908.
van der Klis, M., and Bonnet-Bidaud, J. M. 1984, *Astr. Ap.*, **135**, 155.

P. E. Boynton and J. E. Deeter: Department of Astronomy, University of Washington, Seattle, WA 98195

F. K. Lamb and G. Zylstra: Department of Physics, University of Illinois at Urbana-Champaign, Urbana, IL 61801